

# CD39<sup>+</sup> tissue-resident memory CD8<sup>+</sup> T cells with a clonal overlap across compartments mediate antitumor immunity in breast cancer

Yong Joon Lee<sup>1,2†</sup>, Jee Ye Kim<sup>2†</sup>, Seung Hyuck Jeon<sup>1</sup>, Heejin Nam<sup>1</sup>, Jae Hyung Jung<sup>1</sup>, Minwoo Jeon<sup>1</sup>, Eui-Soon Kim<sup>1</sup>, Soong June Bae<sup>3</sup>, Juneyoung Ahn<sup>4</sup>, Tae-Kyung Yoo<sup>5</sup>, Woo Young Sun<sup>6</sup>, Sung Gwe Ahn<sup>3</sup>, Joon Jeong<sup>3</sup>, Su-Hyung Park<sup>1</sup>, Woo Chan Park<sup>5\*</sup>, Seung Il Kim<sup>2\*</sup>, Eui-Cheol Shin<sup>1\*</sup>

Despite being a standard treatment option in breast cancer, immune checkpoint inhibitors (ICIs) are only efficacious for a subset of patients. To gain a better understanding of the antitumor immune response in breast cancer, we examined the heterogeneity of CD8<sup>+</sup> T cells in tumors, metastatic lymph nodes (mLNs), and peripheral blood from patients with early breast cancer ( $n = 131$ ). Among tissue-resident memory CD8<sup>+</sup> T ( $T_{RM}$ ) cells, including virus- and tumor-specific CD8<sup>+</sup> T cells, CD39 expression was observed in a tumor-specific and exhausted subpopulation in both tumors and mLNs. CD39<sup>+</sup>  $T_{RM}$  cells from tumors and mLNs exhibited a phenotypic similarity and clonally overlapped with each other. Moreover, tumor or mLN CD39<sup>+</sup>  $T_{RM}$  cells clonally overlapped with CD39<sup>−</sup>  $T_{RM}$  and non- $T_{RM}$  cells in the same compartment, implying a tissue-specific differentiation process. These inter-subpopulationally overlapping CD39<sup>+</sup>  $T_{RM}$  clonotypes were frequently detected among effector memory CD8<sup>+</sup> T cells in peripheral blood, suggesting a systemic clonal overlap. CD39<sup>+</sup>  $T_{RM}$  cell enrichment was heterogeneous among molecular subtypes of breast cancer, which is associated with the different role of antitumor immune responses in each subtype. In vitro blockade of PD-1 and/or CTLA-4 effectively restored proliferation of CD39<sup>+</sup>  $T_{RM}$  cells and enhanced cytokine production by CD8<sup>+</sup> T cells from tumors or mLNs, particularly in the presence of CD39<sup>+</sup>  $T_{RM}$  enrichment. This suggests that CD39<sup>+</sup>  $T_{RM}$  cells have a capacity for functional restoration upon ICI treatment. Thus, our study indicates that CD39<sup>+</sup>  $T_{RM}$  cells with a clonal overlap across compartments are key players in antitumor immunity in breast cancer.

## INTRODUCTION

Immune checkpoint inhibitors (ICIs), including programmed cell death protein 1 (PD-1) and programmed death-ligand 1 (PD-L1) blockers, have demonstrated clinical efficacy in patients with advanced or metastatic breast cancer, especially in those with the triple-negative breast cancer (TNBC) subtype (1, 2). In addition, the combination of ICIs with neoadjuvant chemotherapy leads to improved event-free survival and an increased pathological complete response rate in TNBC, suggesting that neoadjuvant ICIs are

a promising treatment option for patients with early breast cancer (3–5). However, the treatment response to ICIs is low in patients with non-TNBC subtypes, which account for >80% of breast cancers (6–8), and the underlying mechanisms are unclear. In addition, the clinical value of immunological markers, including tissue expression of PD-L1 or the abundance of tumor-infiltrating lymphocytes (TILs), has not been defined for predicting ICI treatment responses, indicating that our current knowledge of antitumor immune responses is limited in breast cancer.

Despite being initially considered as poorly immunogenic, breast cancer is an immunologically heterogeneous disease depending on the molecular subtype (9). Higher numbers of TILs have been observed in human epithelial growth factor receptor 2-positive (HER-2<sup>+</sup>) or TNBC subtypes compared with hormone receptor-positive/HER-2-negative (HR<sup>+</sup>/HER-2<sup>−</sup>) subtypes (10, 11). Moreover, the abundance of TILs, especially CD8<sup>+</sup> TILs, has a positive prognostic value only in patients with HER-2<sup>+</sup> or TNBC subtypes (12–15), indicating heterogeneous roles of TILs among molecular subtypes of breast cancer.

Accumulating evidence implies heterogeneity among CD8<sup>+</sup> TILs in human cancers, especially in terms of antigen specificity. Low and variable tumor reactivity of the intratumoral T cell receptor (TCR) repertoire is reported in high-grade ovarian cancer (OVC) and microsatellite stable colorectal cancer (CRC) (16). Tumor-

<sup>1</sup>Graduate School of Medical Science and Engineering, Korea Advanced Institute of Science and Technology, Daejeon 34141, Republic of Korea. <sup>2</sup>Department of Surgery, Yonsei University College of Medicine, Seoul 03722, Republic of Korea. <sup>3</sup>Department of Surgery, Gangnam Severance Hospital, Yonsei University College of Medicine, Seoul 06273, Republic of Korea. <sup>4</sup>Department of Surgery, Uijeongbu St. Mary's Hospital, College of Medicine, Catholic University of Korea, Seoul 11765, Republic of Korea. <sup>5</sup>Department of Surgery, Seoul St. Mary's Hospital, College of Medicine, Catholic University of Korea, Seoul 06591, Republic of Korea. <sup>6</sup>Department of Surgery, Daejeon St. Mary's Hospital, College of Medicine, Catholic University of Korea, Seoul 34943, Republic of Korea. \*Corresponding author. Email: wcpark@catholic.ac.kr (W.C.P.); ecshin@kaist.ac.kr (E.-C.S.); skim@yuhs.ac (S.I.K.)

†These authors contributed equally to this work.

Copyright © 2022

The Authors, some

rights reserved;

exclusive licensee

American Association

for the Advancement

of Science. No claim

to original U.S.

Government Works

nonspecific bystander CD8<sup>+</sup> T cells, including viral antigen-specific CD8<sup>+</sup> T cells, are also abundant in tumor infiltrates from non-small cell lung carcinoma (NSCLC) and CRC (17). In OVC and NSCLC, CD8<sup>+</sup> TILs with phenotypes of tissue-resident memory CD8<sup>+</sup> T (T<sub>RM</sub>) cells, which typically express CD69 and CD103, exhibit more tumor-specific features (18, 19). In breast cancer, CD103<sup>+</sup>CD8<sup>+</sup> TILs are spatially located adjacent to tumor cells and associated with improved prognosis (20, 21). However, no study has comprehensively evaluated the heterogeneity of CD8<sup>+</sup> TILs in the context of tumor specificity and its relationship with the antitumor immune response in breast cancer.

CD39 is a marker for tumor antigen specificity (17, 22–25) or exhaustion (26), especially terminal exhaustion (27, 28). Although these concepts are related, their implications in the antitumor immune response can be interpreted differently. Enrichment of CD39<sup>+</sup>CD8<sup>+</sup> TILs has shown a disparate prognostic importance (22, 23, 29) and different predictive abilities for the response to immune checkpoint blockade (30, 31) depending on the type of cancer. In this context, it is meaningful to characterize the phenotypes and functionalities of CD39<sup>+</sup>CD8<sup>+</sup> T cells in depth and to investigate their importance to prognosis and ICI treatment in breast cancer. In the current study, we examined the heterogeneity of CD8<sup>+</sup> T cells obtained from different compartments, including primary tumors, metastatic lymph nodes (mLNs), and peripheral blood, by recruiting multicenter cohorts of patients with early breast cancer who underwent curative-aimed surgery.

## RESULTS

### CD39 expression enriches a tumor-specific subpopulation of T<sub>RM</sub> cells

We examined the composition of immune cells in peripheral blood and tumor tissues from patients with early breast cancer (*n* = 131) using multicolor flow cytometry (fig. S1A). Among live CD45<sup>+</sup> cells, T cells were the major immune cell subset in tumors (fig. S1B). The percentage of CD8<sup>+</sup> T cells among T cells was significantly higher in tumors than in the peripheral blood (fig. S1C). We examined T<sub>RM</sub> markers, such as CD69 and CD103, on CD8<sup>+</sup> T cells (Fig. 1A). The percentage of CD69<sup>+</sup>CD103<sup>+</sup> T<sub>RM</sub> cells among CD8<sup>+</sup> T cells was significantly higher in tumors than in the peripheral blood (Fig. 1B). CD103 was coexpressed by a subpopulation of CD69<sup>+</sup>CD8<sup>+</sup> T cells in tumors (fig. S1D).

We also examined the antigen specificity of CD8<sup>+</sup> T cells. We detected virus-specific bystander CD8<sup>+</sup> T cells that were unrelated to tumor antigens using human leukocyte antigen (HLA)-A\*02 multimers loaded with human cytomegalovirus (HCMV) pp65<sub>495–503</sub> or influenza A virus (IAV) M1<sub>58–66</sub> peptide (Fig. 1C). Although the percentages of HCMV- or IAV-specific cells among CD8<sup>+</sup> T cells varied across patients (Fig. 1D), the percentage of IAV-specific cells among CD8<sup>+</sup> T cells was significantly increased in tumors compared with peripheral blood, but we found no difference in the percentage of HCMV-specific cells (Fig. 1E). This difference could be explained by the fact that about half of IAV-specific CD8<sup>+</sup> TILs were CD69<sup>+</sup>CD103<sup>+</sup> T<sub>RM</sub> cells, whereas <10% of HCMV-specific CD8<sup>+</sup> TILs were CD69<sup>+</sup>CD103<sup>+</sup> T<sub>RM</sub> cells (Fig. 1F).

Next, we used an HLA-A\*02 multimer loaded with NY-ESO-1<sub>157–165</sub> peptide to detect tumor antigen-specific CD8<sup>+</sup> T cells.

NY-ESO-1 is a cancer-testis antigen that is overexpressed across various types of tumors, including breast cancer, particularly the TNBC subtype (32, 33). NY-ESO-1-specific cells were only detected among CD8<sup>+</sup> TILs from patients with TNBC (fig. S1E) and were simultaneously detected in peripheral blood CD8<sup>+</sup> T cells from certain cases. CD69<sup>+</sup>CD103<sup>+</sup> T<sub>RM</sub> cells were the dominant population in NY-ESO-1-specific CD8<sup>+</sup> TILs but were absent in NY-ESO-1-specific peripheral blood CD8<sup>+</sup> T cells (Fig. 1G). In addition, the percentage of CD69<sup>+</sup>CD103<sup>+</sup> T<sub>RM</sub> cells was significantly increased among NY-ESO-1-specific CD8<sup>+</sup> TILs compared with the total CD8<sup>+</sup> TILs (Fig. 1H and fig. S1F), indicating that CD69<sup>+</sup>CD103<sup>+</sup> T<sub>RM</sub> cells are preferentially enriched in tumor antigen-specific CD8<sup>+</sup> TILs. Because CD103 was expressed exclusively by CD69<sup>+</sup>CD8<sup>+</sup> cells (Fig. 1G and fig. S1D), CD103<sup>+</sup>CD8<sup>+</sup> T cells were regarded as T<sub>RM</sub> cells.

To better define tumor antigen-specific CD8<sup>+</sup> T cells, we stained for CD39, which is a marker of tumor antigen-specific CD8<sup>+</sup> T cells in several types of cancers (17, 22–25). CD39 expression was restricted in CD103<sup>+</sup> T<sub>RM</sub> cells (fig. S1G), and CD39<sup>+</sup>CD103<sup>+</sup> T<sub>RM</sub> cells were observed only in NY-ESO-1-specific CD8<sup>+</sup> TILs but not in IAV- or HCMV-specific CD8<sup>+</sup> TILs (Fig. 1I). We also compared the expression of CD39 between CD8<sup>+</sup> T cells from tumor and tumor-adjacent normal tissues. Although the percentage of CD103<sup>+</sup> T<sub>RM</sub> cells among CD8<sup>+</sup> T cells was not different between tumor and normal tissues, the percentage of CD39<sup>+</sup>CD103<sup>+</sup> T<sub>RM</sub> cells was significantly increased in tumor tissues compared with normal tissues (Fig. 1J). Together, these results indicated that CD39 expression enriches tumor antigen-specific T<sub>RM</sub> cells in breast cancer.

### CD39<sup>+</sup> T<sub>RM</sub> cells are exhausted in both tumors and mLNs

To comprehensively investigate the transcriptomic characteristics of CD39<sup>+</sup>CD103<sup>+</sup> T<sub>RM</sub>, we sorted CD8<sup>+</sup> TILs into three subpopulations to perform bulk mRNA sequencing: CD39<sup>+</sup> T<sub>RM</sub> (CD39<sup>+</sup>CD103<sup>+</sup>), CD39<sup>−</sup> T<sub>RM</sub> (CD39<sup>−</sup>CD103<sup>+</sup>), and non-T<sub>RM</sub> (CD39<sup>−</sup>CD103<sup>−</sup>) cells. Gene clustering analysis showed that CD39<sup>+</sup> T<sub>RM</sub> cells had distinct transcriptomic profiles compared with CD39<sup>−</sup> T<sub>RM</sub> and non-T<sub>RM</sub> cells (Fig. 2A and fig. S2A). CD39<sup>+</sup> T<sub>RM</sub> cells highly expressed *TOX*, the gene encoding a DNA-binding factor that programs T cell exhaustion (34–37), and immune checkpoint-related genes, including *LAYN*, *CXCL13*, *HAVCR2*, and *TIGIT*, compared with CD39<sup>−</sup> T<sub>RM</sub> or non-T<sub>RM</sub> cells. In addition, CD39<sup>+</sup> T<sub>RM</sub> cells exhibited up-regulation of genes related to effector functions, including *GZMB* and *IFNG*, and genes related to T cell activation, including *TNFRSF9*, *HLA-DRA*, and *HLA-DRB1*. In contrast, CD39<sup>+</sup> T<sub>RM</sub> cells exhibited down-regulation of *IL7R* and *CCR7*, which are associated with naïve or central memory CD8<sup>+</sup> T cells, compared with CD39<sup>−</sup> T<sub>RM</sub> or non-T<sub>RM</sub> cells. Gene Ontology (GO) biological pathway analysis revealed cell activation features in CD39<sup>+</sup> T<sub>RM</sub> cells compared with CD39<sup>−</sup> T<sub>RM</sub> cells (Fig. 2B). We also performed gene set enrichment analysis (GSEA) using gene sets from recently identified CD8<sup>+</sup> T cell clusters based on single-cell RNA sequencing (scRNA-seq) analysis in breast cancer (20). Up-regulated genes in the T<sub>RM</sub>-like cluster were enriched in CD39<sup>+</sup> T<sub>RM</sub> cells compared with CD39<sup>−</sup> T<sub>RM</sub> cells, but up-regulated genes in the effector memory T (T<sub>EM</sub>)-like cluster were enriched in CD39<sup>−</sup> T<sub>RM</sub> cells compared with CD39<sup>+</sup> T<sub>RM</sub> cells (Fig. 2C and fig. S2B). GSEA

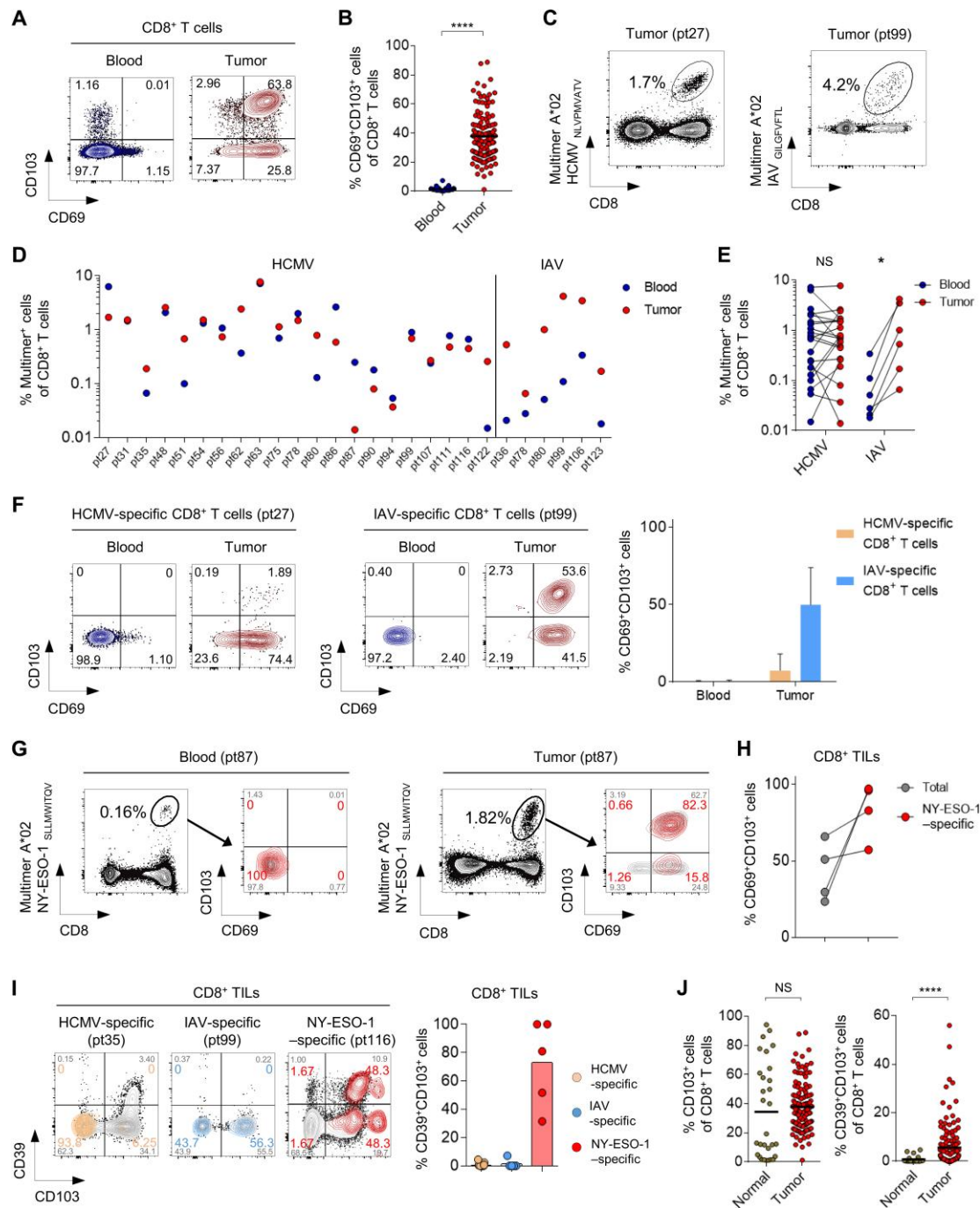


**Fig. 1. CD39 expression enriches a tumor-specific subpopulation of T<sub>RM</sub> cells.** (A and B) Representative flow cytometry plots of T<sub>RM</sub> marker expression (A) and frequencies of CD69<sup>+</sup>CD103<sup>+</sup> cells among CD8<sup>+</sup> T cells (B) in blood ( $n = 122$ ) and tumors ( $n = 131$ ) from patients with breast cancer. Bars represent means. Two-sided unpaired Student's  $t$  test. (C) Representative flow cytometry plots showing ex vivo detection of HLA-A\*02-multimer<sup>+</sup> CD8<sup>+</sup> T cells in two patients. pt, patient. Left: HCMV-specific CD8<sup>+</sup> T cells. Right: IAV-specific CD8<sup>+</sup> T cells. (D and E) Frequencies of HCMV-specific CD8<sup>+</sup> T cells ( $n = 21$ ) or IAV-specific CD8<sup>+</sup> T cells ( $n = 6$ ) identified by multimer staining in blood and tumors. Patient numbers are indicated on the x axis (D). Wilcoxon matched-pairs signed rank test (E). (F) Representative flow cytometry plots of T<sub>RM</sub> marker expression on virus-specific CD8<sup>+</sup> T cells (left) and frequencies of CD69<sup>+</sup>CD103<sup>+</sup> cells among virus-specific CD8<sup>+</sup> T cells in blood or tumors (right): HCMV-specific ( $n = 19$ ) and IAV-specific ( $n = 6$ ). Data are presented as means + SD. (G and H) Ex vivo detection of NY-ESO-1-specific CD8<sup>+</sup> T cells and their expression of T<sub>RM</sub> markers. Representative flow cytometry plots (G) and frequencies of CD69<sup>+</sup>CD103<sup>+</sup> cells among NY-ESO-1-specific CD8<sup>+</sup> TILs or total CD8<sup>+</sup> TILs (H,  $n = 4$ ). Numbers that are colored in red in gating plots indicate the percentages of gated subsets among NY-ESO-1-specific CD8<sup>+</sup> T cells. Numbers that are colored in gray in gating plots indicate the percentages of gated subsets among total CD8<sup>+</sup> T cells. (I) Comparison of CD39 and CD103 expression among multimer<sup>+</sup> CD8<sup>+</sup> TILs (right): HCMV-specific ( $n = 21$ ), IAV-specific ( $n = 5$ ), and NY-ESO-1-specific ( $n = 5$ ). Bars represent means. (J) Frequencies of CD103<sup>+</sup> cells (left) and CD39<sup>+</sup>CD103<sup>+</sup> cells (right) among CD8<sup>+</sup> T cells in normal tissues ( $n = 30$ ) and tumors ( $n = 131$ ). Two-sided unpaired Student's  $t$  test. \* $P \leq 0.05$  and \*\*\*\* $P \leq 0.0001$ . NS, not significant.



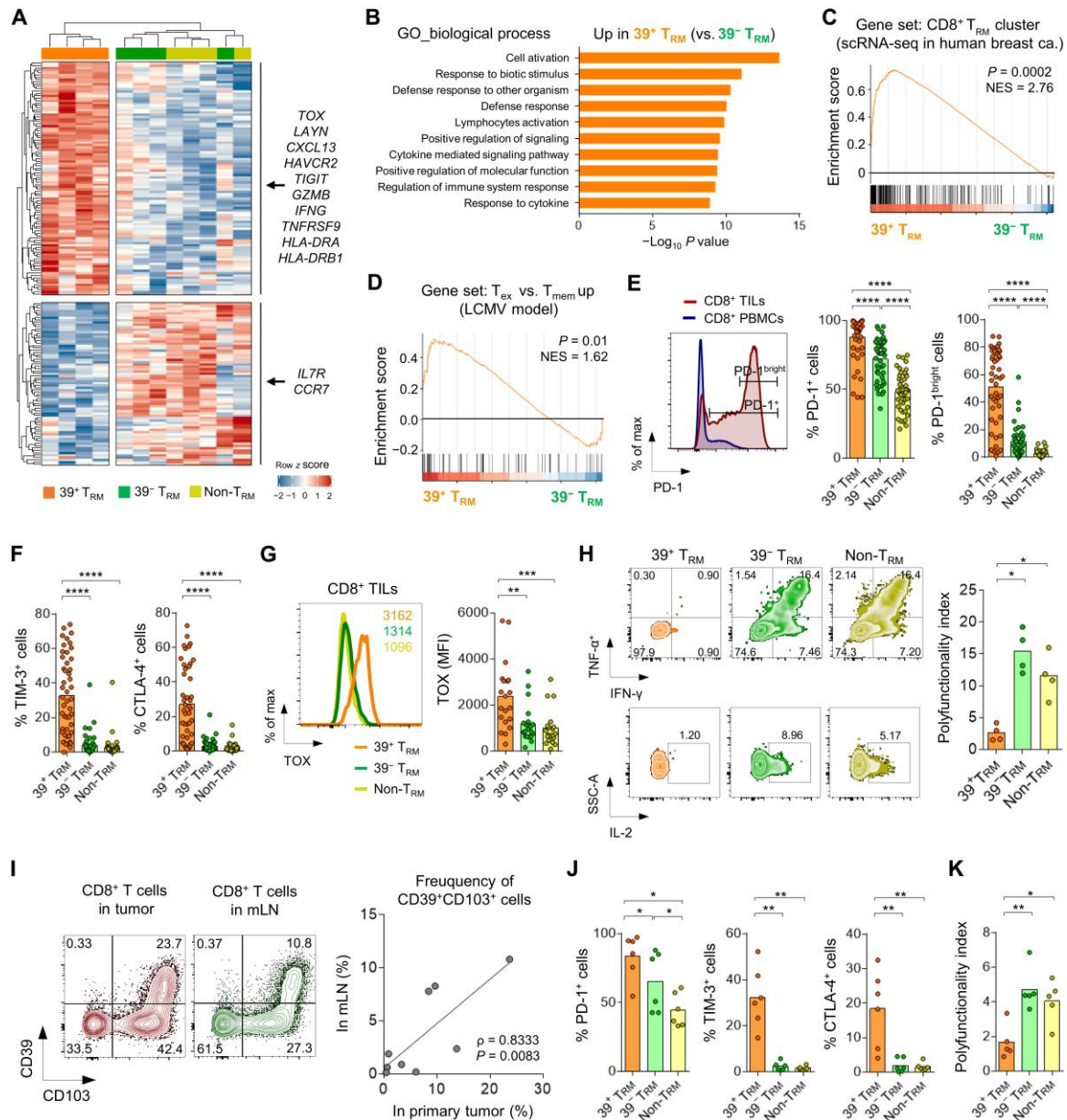
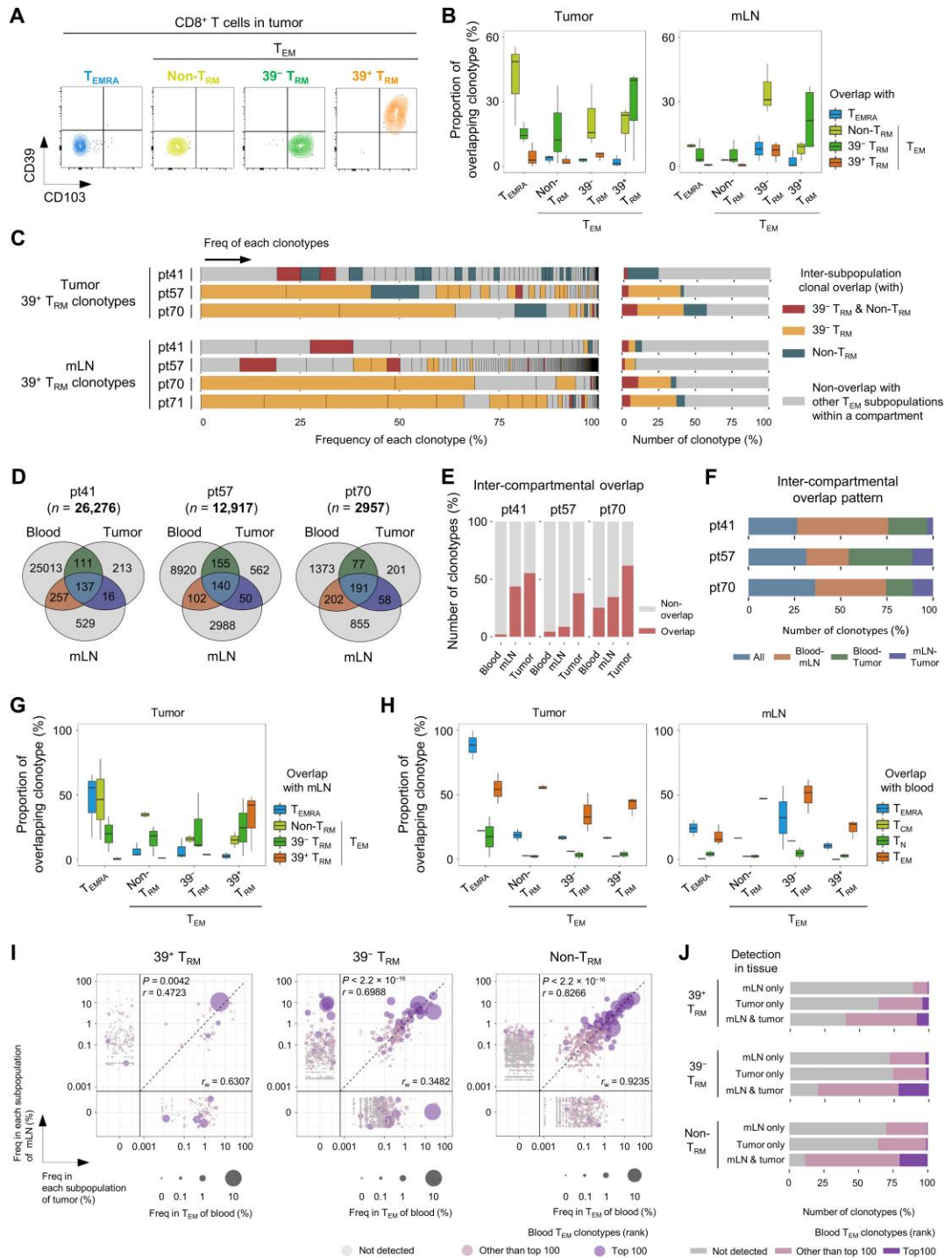


**Fig. 2. CD39<sup>+</sup> T<sub>RM</sub> cells are exhausted in both tumors and mLN.** (A) Heat map comparing gene signatures derived from bulk RNA-seq and unsupervised clustering of the DEGs among three subpopulations of CD8<sup>+</sup> T cells in tumors (HER-2<sup>+</sup>,  $n = 2$ ; TNBC,  $n = 2$ ); CD39<sup>+</sup> T<sub>RM</sub> cells (39<sup>+</sup> T<sub>RM</sub>), CD39<sup>-</sup> T<sub>RM</sub> cells (39<sup>-</sup> T<sub>RM</sub>), and non-T<sub>RM</sub> cells (Non-T<sub>RM</sub>). (B) Bar plots showing enrichment  $P$  values for the top 10 GO biological pathways in CD39<sup>+</sup> T<sub>RM</sub> cells for up-regulated genes compared with CD39<sup>-</sup> T<sub>RM</sub> cells. (C and D) GSEA of CD8<sup>+</sup> T<sub>RM</sub> cluster gene sets from previous scRNA-seq data for human breast cancer (20) (C) or up-regulated gene sets in exhausted T cells versus memory T cells from a mouse LCMV model (38) (D) in CD39<sup>+</sup> T<sub>RM</sub> and CD39<sup>-</sup> T<sub>RM</sub> cells. NES, normalized enrichment score. (E) Representative flow cytometry plot of PD-1 expression on CD8<sup>+</sup> T cell subpopulations in blood or tumors (left). PD-1<sup>bright</sup> is defined by higher expression of PD-1 on CD8<sup>+</sup> T cells in tumors than the expression level of PD-1 on CD8<sup>+</sup> T cells in blood. Frequencies of PD-1<sup>+</sup> cells or PD-1<sup>bright</sup> cells among each fraction (middle and right,  $n = 46$ ). Bars represent means. Two-sided unpaired Student's  $t$  test. (F) Frequencies of TIM-3<sup>+</sup> cells and CTLA-4<sup>+</sup> cells among CD8<sup>+</sup> T cell subpopulations in tumors ( $n = 46$ ). Bars represent means. Two-sided unpaired Student's  $t$  test. (G) Representative flow cytometry plot of TOX expression (left) and the expression levels of TOX on CD8<sup>+</sup> T cell subpopulations in tumors (right,  $n = 20$ ). Values inside the plot indicate the median fluorescence intensity (MFI) of TOX. Bars represent means. Two-sided unpaired Student's  $t$  test. (H) Tumor lysates were stimulated with anti-CD3 antibody (1  $\mu$ g/ml) for 6 hours and intracellular cytokine staining performed. Representative flow cytometry plots showing cytokine production by CD8<sup>+</sup> T cell subpopulations upon anti-CD3 stimulation (left). A polyfunctionality index was calculated using a formula that accounted for the combinatorial production of IFN- $\gamma$ , TNF- $\alpha$ , and IL-2 (right,  $n = 4$ ) (39). Bars represent means. Mann-Whitney test. (I) Comparison of CD39 expression and CD103 expression on CD8<sup>+</sup> T cells between tumors and mLN. Left: Representative flow cytometry plots from a patient. Right: Association of frequencies of CD39<sup>+</sup>CD103<sup>+</sup> cells among CD8<sup>+</sup> T cells between primary tumors and paired mLN ( $n = 9$ ).  $\rho$  denotes Spearman correlation.  $P$  value obtained from two-sided  $t$  tests. (J) Frequencies of PD-1<sup>+</sup> cells, TIM-3<sup>+</sup> cells, and CTLA-4<sup>+</sup> cells in CD8<sup>+</sup> T cell subpopulations in mLN ( $n = 6$ ). Bars represent means. Mann-Whitney test. (K) mLN lysates were stimulated with anti-CD3 antibody (1  $\mu$ g/ml) for 6 hours and intracellular cytokine staining performed ( $n = 5$ ). Bars represent means. Mann-Whitney test. \* $P \leq 0.05$ , \*\* $P \leq 0.01$ , \*\*\* $P \leq 0.001$ , and \*\*\*\* $P \leq 0.0001$ . SSC-A, side scatter area.

### Fig. 3. CD39<sup>+</sup> T<sub>RM</sub> cells clonally overlap with other CD8<sup>+</sup> T cell subpopulations within the same compartment.

Clonal analysis of CD8<sup>+</sup> T cells in various compartments, including blood, mLN, and tumors. A CDR3 sequence of the TCR- $\beta$  chain was considered a clonotype of CD8<sup>+</sup> T cells. (A) Sorting strategy for CD8<sup>+</sup> T cells in tumors or mLN for TCR-seq. Detailed information on sorting is given in fig. S3 (A to E) and table S1. (B) Proportion of clonotypes in each CD8<sup>+</sup> T cell subpopulation that overlapped with other subpopulations in the same compartment: tumor (left,  $n = 3$ ) and mLN (right,  $n = 4$ ). Box plots show the median, box edges represent the first and third quartiles, and the whiskers extend to 1.5 $\times$  the interquartile range. (C) Tumor CD39<sup>+</sup> T<sub>RM</sub> clonotypes (top) and mLN CD39<sup>+</sup> T<sub>RM</sub> clonotypes (bottom). Bar plots for each patient (left) show the frequencies of each clonotype among the total CD39<sup>+</sup> T<sub>RM</sub> clonotypes in each compartment. Each clonotype is colored according to the pattern of inter-subpopulation clonal overlap. Bar plots for each patient (right) show the proportions of clonotypes by the pattern of inter-subpopulation clonal overlap. (D to F) Venn diagram for each patient (D) showing the shared clonotypes across compartments. Values below patient numbers indicate the total number of unique clonotypes detected among all compartments for each patient. Values in the Venn diagram indicate the numbers of unique clonotypes in each compartment or shared clonotypes among compartments in the overlapping regions. Bar plots for each patient (E) show the proportions of clonotypes in each compartment by the inter-compartmental clonal overlap. Bar plots for each patient (F) show the proportions of shared clonotypes among compartments by the pattern of inter-compartmental clonal overlap. (G and H) Proportion of clonotypes in each CD8<sup>+</sup> T cell subpopulation of tumors that overlapped with CD8<sup>+</sup> T cell subpopulations of mLN (G,  $n = 3$ ). Proportion of clonotypes in each CD8<sup>+</sup> T cell subpopulation of tumors (left,  $n = 3$ ) and mLN (right,  $n = 3$ ) that overlapped with CD8<sup>+</sup> T cell subpopulations in blood (H). Box plots show the median, box edges represent the first and third quartiles, and the whiskers extend to 1.5 $\times$  the interquartile range. (I and J) Scatter plots (I) showing each distinct clonotype from three patients: CD39<sup>+</sup> T<sub>RM</sub> clonotypes in tumors or mLN (left), CD39<sup>+</sup> T<sub>RM</sub> clonotypes in tumors or mLN (middle), and non-T<sub>RM</sub> clonotypes in tumors or mLN (right). Dots are sized for frequency and colored according to presence or rank in the T<sub>EM</sub> subpopulation of blood. Diagonal lines indicate equal frequencies of clonotypes in tumors and mLN. Horizontal and vertical lines separate the absence and presence of clonotypes within compartments.  $r$  denotes Pearson correlation coefficient on frequencies of clonotypes detected in both tumors and mLN.  $P$  values obtained from two-sided  $t$  tests.  $r_w$  denotes Pearson correlation coefficient, weighted by ( $10^{-7} + \text{frequencies in T}_{EM}$  subpopulation of blood), for frequencies of clonotypes detected in both tumor and mLN. Bar plots (J) show proportions of tumor or mLN clonotypes by presence or rank in the T<sub>EM</sub> subpopulation in blood.



also revealed that up-regulated genes in exhausted CD8<sup>+</sup> T cells from a mouse model of chronic lymphocytic choriomeningitis virus (LCMV) infection, which is a prototype of T cell exhaustion, were enriched in CD39<sup>+</sup> T<sub>RM</sub> cells compared with CD39<sup>-</sup> T<sub>RM</sub> or non-T<sub>RM</sub> cells (Fig. 2D and fig. S2C) (38).

Flow cytometric analysis of TILs confirmed the results of the transcriptomic analysis. The frequencies of PD-1<sup>+</sup> and PD-1<sup>bright</sup> cells were significantly higher in CD39<sup>+</sup> T<sub>RM</sub> cells than in CD39<sup>-</sup> T<sub>RM</sub> and non-T<sub>RM</sub> cells and were significantly higher in CD39<sup>-</sup> T<sub>RM</sub> cells than in non-T<sub>RM</sub> cells (Fig. 2E). The frequencies of T-cell immunoglobulin and mucin-domain containing-3 (TIM-3)<sup>+</sup> and cytotoxic T-lymphocyte-associated protein 4 (CTLA-4)<sup>+</sup> cells were also significantly higher in CD39<sup>+</sup> T<sub>RM</sub> cells than in CD39<sup>-</sup> T<sub>RM</sub> and non-T<sub>RM</sub> cells (Fig. 2F). Moreover, the expression of TOX was significantly higher in CD39<sup>+</sup> T<sub>RM</sub> cells than in CD39<sup>-</sup> T<sub>RM</sub> or non-T<sub>RM</sub> cells (Fig. 2G). Upon anti-CD3 stimulation, CD39<sup>+</sup> T<sub>RM</sub> cells produced interferon- $\gamma$  (IFN- $\gamma$ ), tumor necrosis factor- $\alpha$  (TNF- $\alpha$ ), and interleukin-2 (IL-2) to a lesser extent than CD39<sup>-</sup> T<sub>RM</sub> or non-T<sub>RM</sub> cells (Fig. 2H and fig. S2, D and E). Analysis of the polyfunctionality index (39), which scores the ability to simultaneously produce multiple cytokines, yielded similar results, confirming that CD39<sup>+</sup> T<sub>RM</sub> cells are functionally exhausted (Fig. 2H).

Next, we examined whether the characteristics of CD39<sup>+</sup> T<sub>RM</sub> cells found in primary tumors are also observed in paired mLN tissues (Fig. 2I). Tumor metastasis to LNs was confirmed by intra-operative frozen section examination. The frequencies of CD39<sup>+</sup> T<sub>RM</sub> cells in primary tumors closely correlated with the frequencies of CD39<sup>+</sup> T<sub>RM</sub> cells in paired mLN tissues. In addition, the transcriptional characteristics of mLN CD39<sup>+</sup> T<sub>RM</sub> cells and tumor CD39<sup>+</sup> T<sub>RM</sub> cells were similar to each other but distinct from CD39<sup>-</sup> T<sub>RM</sub> cells and non-T<sub>RM</sub> cells (fig. S2F). Among CD8<sup>+</sup> T cells from mLNs, CD39<sup>+</sup> T<sub>RM</sub> cells exhibited a significantly higher frequency of PD-1<sup>+</sup>, TIM-3<sup>+</sup>, and CTLA-4<sup>+</sup> cells than CD39<sup>-</sup> T<sub>RM</sub> and non-T<sub>RM</sub> cells (Fig. 2J). In addition, anti-CD3-induced polyfunctionality was significantly reduced in CD39<sup>+</sup> T<sub>RM</sub> cells compared with CD39<sup>-</sup> T<sub>RM</sub> and non-T<sub>RM</sub> cells among CD8<sup>+</sup> T cells from mLNs, confirming that CD39<sup>+</sup> T<sub>RM</sub> cells in mLNs share a common feature with CD39<sup>+</sup> T<sub>RM</sub> cells in primary tumors (Fig. 2K). These data suggested that CD39<sup>+</sup> T<sub>RM</sub> cells in both tumors and mLNs were exhausted.

### CD39<sup>+</sup> T<sub>RM</sub> cells clonally overlap with other CD8<sup>+</sup> T cell subpopulations within the same compartment

To examine the clonality of CD39<sup>+</sup> T<sub>RM</sub> cells, we performed TCR analysis. To comprehensively compare CD8<sup>+</sup> T cells among different compartments (i.e., primary tumors, mLNs, and peripheral blood), we sorted CD8<sup>+</sup> T cells into various CD8<sup>+</sup> T cell subpopulations and performed RNA-based bulk TCR sequencing (TCR-seq). We defined CD8<sup>+</sup> T cell subsets using CCR7 and CD45RA according to the standard classification of human CD8<sup>+</sup> T cells (40–42). CD8<sup>+</sup> T cells were primarily sorted into CCR7<sup>+</sup>CD45RA<sup>+</sup> naïve (T<sub>N</sub>), CCR7<sup>+</sup>CD45RA<sup>-</sup> central memory T (T<sub>CM</sub>), CCR7<sup>-</sup>CD45RA<sup>-</sup> T<sub>EM</sub>, and CCR7<sup>-</sup>CD45RA<sup>+</sup> terminally differentiated effector memory T (T<sub>EMRA</sub>) cells (fig. S3A). In tumors and mLNs, T<sub>EM</sub> cells were the predominant population (fig. S3B), and CD103<sup>+</sup> T<sub>RM</sub> cells were largely detected in the T<sub>EM</sub> population (fig. S3, C and D). Accordingly, we further sorted tumor or mLN T<sub>EM</sub> cells

into CD39<sup>+</sup> T<sub>RM</sub>, CD39<sup>-</sup> T<sub>RM</sub>, and non-T<sub>RM</sub> cells (Fig. 3A, fig. S3E, and table S1).

We analyzed the CDR3 sequences of the TCR-beta chains and found that tumor or mLN CD39<sup>+</sup> T<sub>RM</sub> cells were not clonally distinct but overlapped with other subpopulations within the same compartment, indicating that clonally identical CD8<sup>+</sup> T cells exhibited a heterogeneous differentiation status within tumors or mLNs (Fig. 3B and fig. S4, A to C). Depending on the sample, >50% of CD39<sup>+</sup> T<sub>RM</sub> clonotypes, including high-rank clonotypes, overlapped with CD39<sup>-</sup> T<sub>RM</sub> or non-T<sub>RM</sub> clonotypes within the same compartment (Fig. 3C).

We further examined the possibility that a sorted cell population could have been contaminated by unwanted cells and evaluated whether our TCR clonotype results were affected by contamination with minor clonotypes. We analyzed the ranks of clonotypes with inter-subpopulational overlap in each subpopulation under the assumption that clonotypes with inter-subpopulational overlap would be found as low-ranked clonotypes if they originated from contaminating minor cells. Consequently, CD39<sup>+</sup> T<sub>RM</sub> clonotypes with inter-subpopulational overlap were not enriched among low-ranked clonotypes (fig. S5A). Similar results were observed when CD39<sup>-</sup> T<sub>RM</sub> (fig. S5B) and non-T<sub>RM</sub> (fig. S5C) clonotypes were analyzed. These results indicated minimal effects of contaminating minor clonotypes on our TCR clonotype analysis.

Next, we examined whether a CD8<sup>+</sup> T cell clonal connection existed among different compartments. Investigation of the inter-compartmental overlap of CD8<sup>+</sup> T cell clonotypes showed that a considerable proportion (9 to 62%) of clonotypes from tumors or mLNs were also detected in other compartments (Fig. 3, D and E). Moreover, >80% of intercompartmentally overlapping clonotypes were detected in the peripheral blood (Fig. 3F), implying the presence of a CD8<sup>+</sup> T cell clonal connection between local tissue compartments and systemic blood. Intercompartmental clonal overlaps between tissue compartments were largely observed between the same subpopulations of each compartment; for example, 6 to 49% of tumor CD39<sup>+</sup> T<sub>RM</sub> clonotypes overlapped with mLN CD39<sup>+</sup> T<sub>RM</sub> clonotypes (Fig. 3G and fig. S5D). In addition, clonotypes of T<sub>EM</sub> cells in tumors or mLNs, including CD39<sup>+</sup> T<sub>RM</sub>, CD39<sup>-</sup> T<sub>RM</sub>, and non-T<sub>RM</sub> cells, mostly overlapped with T<sub>EM</sub> clonotypes in peripheral blood (Fig. 3H and fig. S5E). Overlapping CD39<sup>+</sup> T<sub>RM</sub> clonotypes between tumors and mLNs were frequently detected in blood T<sub>EM</sub> clonotypes, whereas nonoverlapping CD39<sup>+</sup> T<sub>RM</sub> clonotypes were minor or undetectable in the blood (Fig. 3, I and J). Furthermore, overlapping CD39<sup>-</sup> T<sub>RM</sub> or non-T<sub>RM</sub> clonotypes between tumors and mLNs were readily detected in blood T<sub>EM</sub> clonotypes, whereas nonoverlapping CD39<sup>-</sup> T<sub>RM</sub> or non-T<sub>RM</sub> clonotypes were less easily detected in the blood. Together, these findings suggested a CD8<sup>+</sup> T cell clonal overlap across different compartments, including local tissues and peripheral blood.

### Tissue CD39<sup>+</sup> T<sub>RM</sub> clonotypes with inter-subpopulational overlap are systemically overlapping clonotypes

As described above, tumor or mLN CD39<sup>+</sup> T<sub>RM</sub> cells clonally overlapped with blood T<sub>EM</sub> cells that did not include CD39<sup>+</sup> cells. We further analyzed the clonal connection between peripheral blood and tumors or mLNs. Large clonotypes in blood T<sub>EM</sub> cells, such as the top 100 clonotypes, were detected in considerable numbers in tissue compartments (fig. S6A). We examined the subpopulation



distribution of overlapping clonotypes in tumors and mLNs and found that both the top 100 and other blood  $T_{EM}$  clonotypes were distributed among various  $CD8^+$  T cell subpopulations in tumors and mLNs, including  $CD39^- T_{RM}$  or  $CD39^+ T_{RM}$  cells, suggesting that blood  $T_{EM}$  cells may differentiate to  $CD39^- T_{RM}$  or  $CD39^+ T_{RM}$  cells in tumors and mLNs (fig. S6, B to D).

We further examined whether inter-subpopulationally overlapping clones in tumors or mLNs were readily detected in other compartments. We classified tumor  $CD39^+ T_{RM}$  clonotypes into inter-subpopulationally overlapping and nonoverlapping clones and tracked these clones into other compartments. In particular, we analyzed the ranks of these clones in blood  $T_{EM}$  cells and the subpopulation distribution in mLNs (Fig. 4A). We also performed a similar analysis using mLN  $CD39^+ T_{RM}$  clonotypes (Fig. 4B). Tumor  $CD39^+ T_{RM}$  clonotypes with inter-subpopulation clonal overlap were more readily detected in blood  $T_{EM}$  cells as large clones than those without inter-subpopulation clonal overlap (Fig. 4C). In addition, tumor  $CD39^+ T_{RM}$  clonotypes with inter-subpopulation clonal overlap were distributed among various subpopulations in mLNs, whereas those without inter-subpopulation clonal overlap had a restricted subpopulation distribution in mLNs. Similar results were observed in the analysis of mLN  $CD39^+ T_{RM}$  clonotypes with or without inter-subpopulation clonal overlap (Fig. 4D). Tumor or mLN  $CD39^+ T_{RM}$  clonotypes with inter-subpopulation clonal overlap existed as  $CD39^+ T_{RM}$  clonotypes with inter-subpopulation clonal overlap in the other tissues (Fig. 4, E and F). Given the tissue-resident property of  $T_{RM}$  cells, it could be inferred that blood  $T_{EM}$  cells underwent a differentiation process to  $CD39^+ T_{RM}$  cells in both tumors and mLNs.

Collectively, we concluded that tumor or mLN  $CD39^+ T_{RM}$  clones, especially those with with inter-subpopulation clonal overlap, were not compartmentalized but systemically connected across blood and other tissues. Next, we asked whether  $CD39^+ T_{RM}$  cells recognized tumor antigens. To this end, we cocultured sorted mLN  $CD39^+ T_{RM}$  cells with autologous epithelial cell adhesion molecule (EPCAM)<sup>+</sup> cells sorted from tumor single-cell suspensions and examined the up-regulation of 4-1BB, an activation-induced marker, to detect tumor-reactive  $CD39^+ T_{RM}$  cells. We found that the frequency of 4-1BB<sup>+</sup> cells was increased by coculturing with tumor EPCAM<sup>+</sup> cells (Fig. 4G). We further sorted tumor-reactive 4-1BB<sup>+</sup> $CD39^+ T_{RM}$  cells, performed TCR-seq analysis, and mapped 4-1BB<sup>+</sup> $CD39^+ T_{RM}$  clonotypes to mLN  $CD39^+ T_{RM}$  clonotypes from the same patient (pt57). In a clonal tracking analysis, tumor-reactive 4-1BB<sup>+</sup> $CD39^+ T_{RM}$  clonotypes with inter-subpopulation clonal overlap were readily detected in blood  $T_{EM}$  cells as large clones and broadly distributed among various subpopulations in tumors compared with those without inter-subpopulation clonal overlap (Fig. 4H). This result demonstrated that tissue  $CD39^+ T_{RM}$  clonotypes, including tumor antigen-specific TCR clones, were systemically overlapping clonotypes.

### The $CD39^+ T_{RM}$ signature is enriched in TNBC and predicts patient survival

Because tumor  $CD39^+ T_{RM}$  cells exhibited systemically overlapping clonotypes with tumor reactivity, we examined the enrichment of  $CD39^+ T_{RM}$  cells and the  $CD39^+ T_{RM}$  gene signature in tumor tissues among the molecular subtypes of early breast cancer, including  $HR^+/HER-2^-$ ,  $HER-2^+$ , and TNBC (Fig. 5A and table S2).

Although the percentages of  $CD8^+$  cells among  $CD3^+$  TILs and  $CD103^+ T_{RM}$  cells among  $CD8^+$  TILs were not significantly different for different subtypes, the percentage of  $CD39^+ T_{RM}$  cells among  $CD8^+$  TILs was highest in TNBC tumors and lowest in  $HR^+/HER-2^-$  tumors (Fig. 5B). The frequencies of  $CD39^+ T_{RM}$  cells were not affected by other clinical characteristics, including tumor Ki-67 expression, neoadjuvant chemotherapy, pathological tumor stage, and LN metastasis (fig. S7, A to D). When we counted patients with >10%  $CD39^+ T_{RM}$  cells among  $CD8^+$  TILs as  $CD39^+ T_{RM}$  cell-enriched cases, 36.4% of patients with TNBC were  $CD39^+ T_{RM}$  cell-enriched cases, whereas 6.7 and 14.8% of patients with  $HR^+/HER-2^-$  and  $HER-2^+$  were  $CD39^+ T_{RM}$  cell-enriched cases, respectively (Fig. 5C). These results indicated that enrichment of  $CD39^+ T_{RM}$  cells in tumor tissues was different among molecular subtypes of breast cancer, with the highest enrichment in TNBC.

To substantiate our findings in large independent cohorts, we extracted a gene set called the  $CD39^+ T_{RM}$  signature that comprised 48 genes that were significantly up-regulated in  $CD39^+ T_{RM}$  cells compared with  $CD39^- T_{RM}$  cells from our bulk RNA-seq data and applied it to public datasets (table S3). Using gene expression data from the Molecular Taxonomy of Breast Cancer International Consortium (METABRIC) consortium (43), we evaluated enrichment of the  $CD39^+ T_{RM}$  signature among normal breast tissues and primary breast tumors. Consistent with data from flow cytometry, enrichment scores for the  $CD39^+ T_{RM}$  signature in primary tumors were highest in TNBC tumors and lowest in  $HR^+/HER-2^-$  tumors or normal breast tissues (Fig. 5D). These findings were recapitulated in an analysis using gene expression data from the Cancer Genome Atlas (TCGA) dataset (Fig. 5E). Moreover, high enrichment of the  $CD39^+ T_{RM}$  signature in TNBC subtypes compared with  $HR^+/HER-2^-$  subtypes was observed in a metastatic tissue cohort of breast cancer (Fig. 5F) (44).

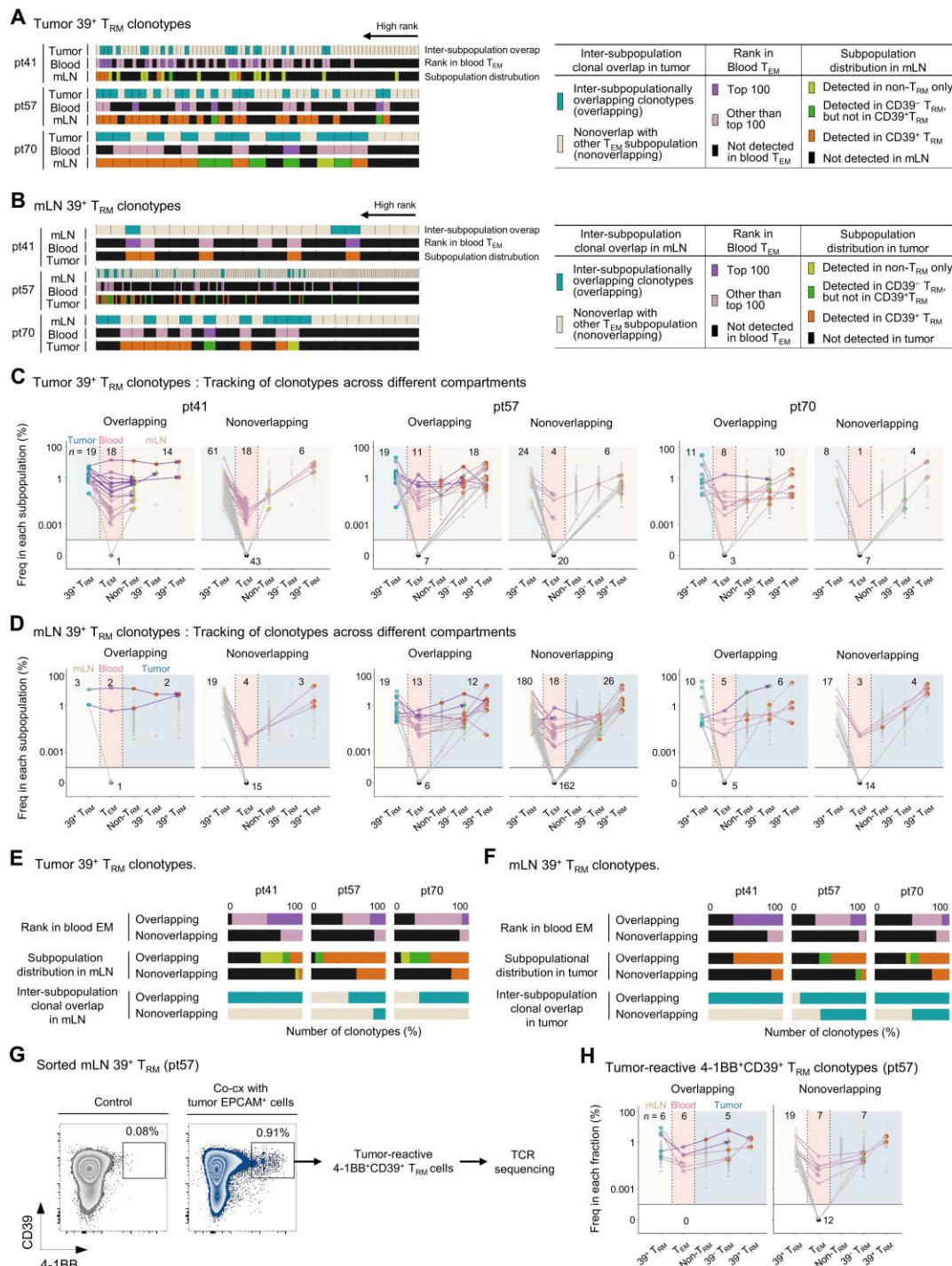
Next, we investigated whether the enrichment score for the  $CD39^+ T_{RM}$  signature in tumors was associated with the survival of patients with breast cancer. To this end, we investigated the prognostic power of the  $CD39^+ T_{RM}$  signature using the METABRIC dataset of primary breast tumors. Among patients with  $HR^+/HER-2^-$  or  $HER-2^+$  tumors, cancer-specific survival was not different between patients with high and low scores for the  $CD39^+ T_{RM}$  signature (Fig. 5G). However, among patients with TNBC subtypes, those with a high  $CD39^+ T_{RM}$  signature score had significantly better cancer-specific survival than those with a low  $CD39^+ T_{RM}$  signature score. Thus, enrichment of a  $CD39^+ T_{RM}$  feature that was different among molecular subtypes predicted the prognosis of patients with TNBC, indicating that  $CD39^+ T_{RM}$  cells directly contribute to antitumor immune responses.

### $CD39^+ T_{RM}$ cells are reinvigorated by blockade of PD-1 and CTLA-4 in vitro

Last, we investigated whether tumor  $CD39^+ T_{RM}$  cells could be reinvigorated by the blockade of immune checkpoint receptors. We performed ex vivo functional assays of  $CD8^+$  TILs in the absence or presence of ICIs. We sorted  $CD8^+$  TILs from a patient with TNBC who was confirmed to have NY-ESO-1-specific  $CD8^+$  TILs and stimulated them ex vivo with NY-ESO-1 overlapping peptides (OLPs) in the presence of autologous irradiated (3000 gray)  $CD8$ -depleted tumor single-cell suspension. We confirmed PD-L1

**Fig. 4. Tissue CD39<sup>+</sup> T<sub>RM</sub> clonotypes with inter-subpopulational overlap are systemically overlapping clonotypes.** Clonal tracking of tissue CD39<sup>+</sup> T<sub>RM</sub> clonotypes across compartments in three patients (pt41, pt57, and pt70). (A) Classification of tumor CD39<sup>+</sup> T<sub>RM</sub> clonotypes in tumors, blood, and mLN

(right). Tumor CD39<sup>+</sup> T<sub>RM</sub> clonotypes were classified according to inter-subpopulation clonal overlap in tumors, their presence or rank in blood T<sub>EM</sub> subpopulations, and their presence or subpopulation distribution in mLNs. Bar plots (left) show tumor CD39<sup>+</sup> T<sub>RM</sub> clonotypes arranged by their rank. In three bar plots for each patient, bars at the same position represent the classification of an identical clonotype in each compartment. (B) Classification of mLN CD39<sup>+</sup> T<sub>RM</sub> clonotypes in mLN, blood, and tumors (right) and bar plots showing mLN CD39<sup>+</sup> T<sub>RM</sub> clonotypes (left). The classification was determined in a similar way as in (A). (C and D) Tracking of tumor CD39<sup>+</sup> T<sub>RM</sub> clonotypes (C) or mLN CD39<sup>+</sup> T<sub>RM</sub> clonotypes (D) across different compartments. Horizontal lines separate the absence and presence of clonotypes within a compartment. Values in the graph indicate the numbers of clonotypes detected in each compartment. Dots represent the frequencies of clonotypes and are colored by the classification of clonotypes in each subpopulation. Small gray dots in the graph indicate the frequencies of total clonotypes in each subpopulation. Identical clonotypes are connected by lines, which are colored by their presence or rank in blood T<sub>EM</sub> subpopulations, across compartments. (E) Bar plots for each patient show the proportions of inter-subpopulationally overlapping or non-overlapping tumor CD39<sup>+</sup> T<sub>RM</sub> clonotypes by the presence or rank in the blood T<sub>EM</sub> subpopulation (top), subpopulation distribution in mLN (middle), and inter-subpopulation clonal overlap in mLN (bottom). (F) Bar plots for each patient show the proportions of inter-subpopulationally overlapping or nonoverlapping mLN CD39<sup>+</sup> T<sub>RM</sub> clonotypes by presence or rank in the blood EM subpopulation (top), subpopulation distribution in tumors (middle), and inter-subpopulation clonal overlap in tumors (bottom). (G and H) Detection of CD39<sup>+</sup> T<sub>RM</sub> clonotypes reactive to autologous tumor cells (G). Fluorescence-activated cell sorting–sorted mLN CD39<sup>+</sup> T<sub>RM</sub> cells were cultured for expansion for 2 weeks and then cocultured with autologous tumor EPCAM<sup>+</sup> cells. Tumor reactivity was confirmed by measuring 4-1BB<sup>+</sup> cells after coculture. Tumor-reactive clonotypes were obtained by TCR-seq of sorted 4-1BB<sup>+</sup>CD39<sup>+</sup> T<sub>RM</sub> cells. Tumor-reactive 4-1BB<sup>+</sup>CD39<sup>+</sup> T<sub>RM</sub> clonotypes were mapped to the mLN CD39<sup>+</sup> T<sub>RM</sub> clonotype from the identical patient (pt57) and tracked across different compartments (H).





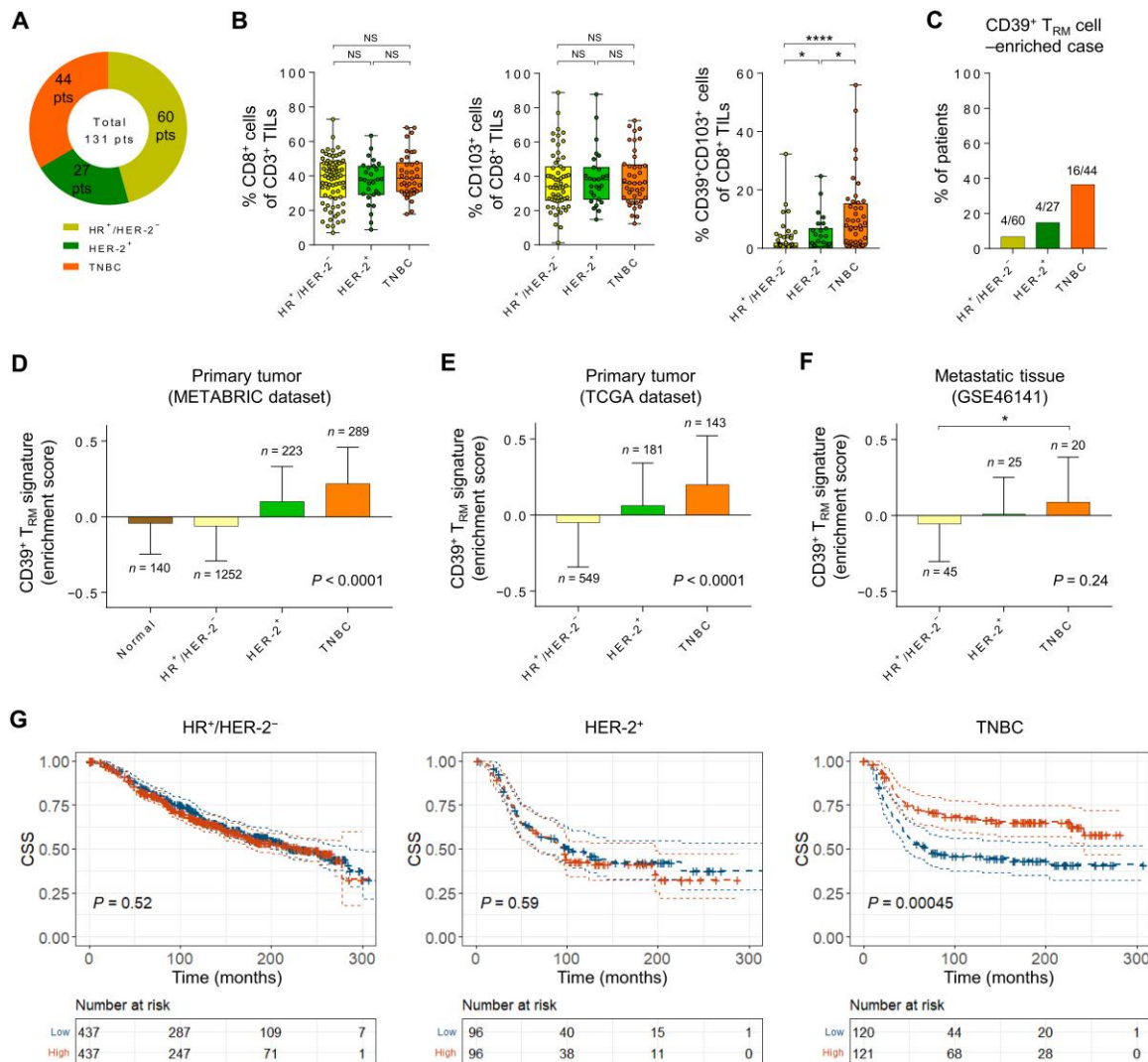
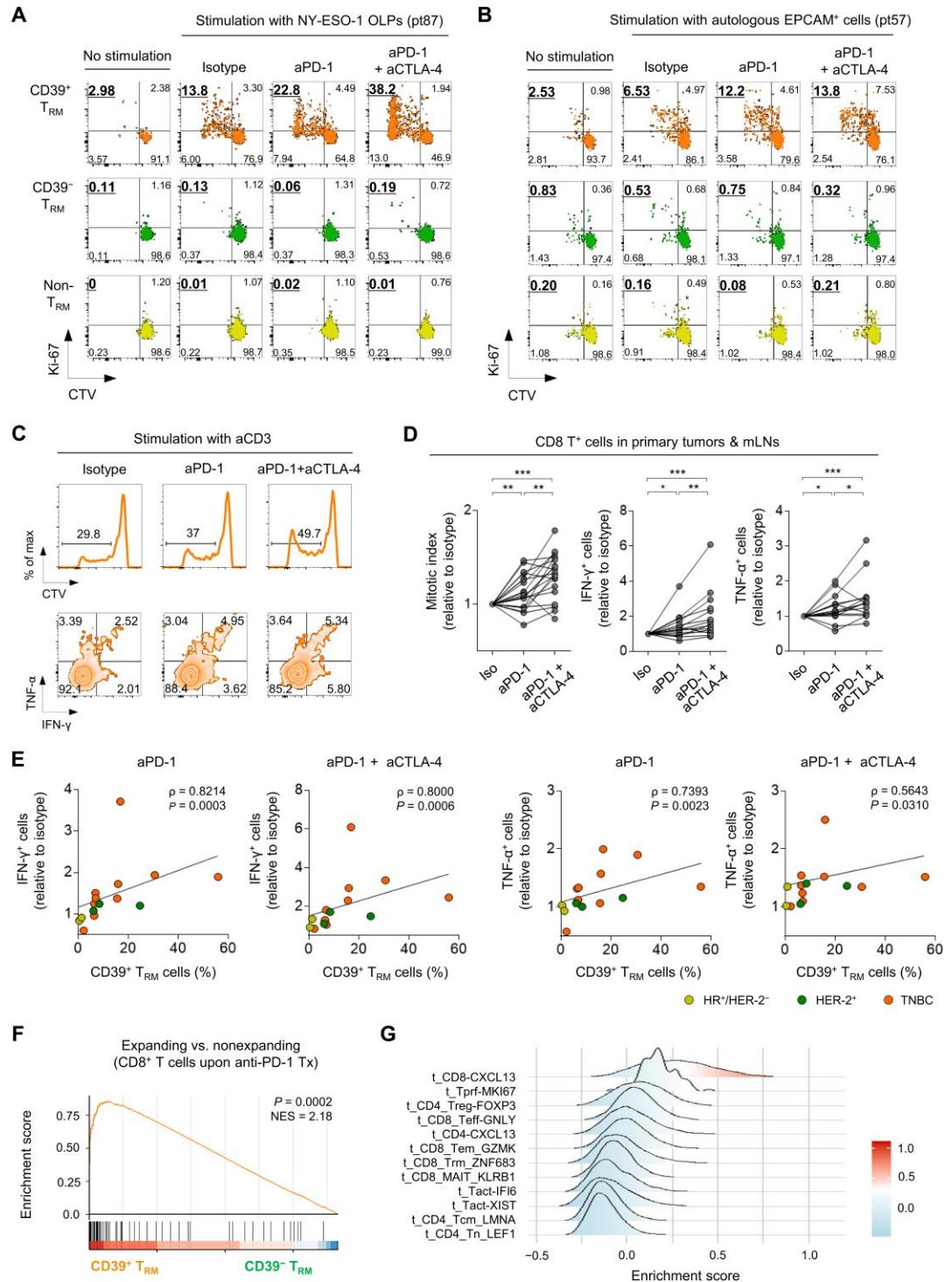


**Fig. 5. The CD39<sup>+</sup> T<sub>RM</sub> signature is enriched in TNBC and predicts patient survival.** (A) Patient statistics according to molecular subtype of breast cancer (n = 131). pts, patients. (B) Frequencies of CD8<sup>+</sup> T cells among CD3<sup>+</sup> TILs (left), CD103<sup>+</sup> cells among CD8<sup>+</sup> TILs (middle), and CD39<sup>+</sup>CD103<sup>+</sup> cells among CD8<sup>+</sup> TILs (right). Box plots show the median, box edges represent the first and third quartiles, and the whiskers extend to the minimum or maximum. Two-sided unpaired Student's t test. (C) Proportions of CD39<sup>+</sup> T<sub>RM</sub> cell-enriched cases, which were defined by >10% CD39<sup>+</sup> T<sub>RM</sub> cells among CD8<sup>+</sup> TILs in each subtype. The text above the bar indicates the number of CD39<sup>+</sup> T<sub>RM</sub> cell-enriched cases divided by the number of total patients. (D–F) Box plot showing the relative enrichment of the CD39<sup>+</sup> T<sub>RM</sub> signature in each subtype. Results were derived from the publicly available METABRIC (43) dataset for primary tumors (D, n = 1904), TCGA dataset for primary tumors (E, n = 873), and GSE46141 (44) dataset for metastatic tumors (F, n = 90). Box plots show the means and SD. Values above the box indicate the numbers of each subtype. Statistical analysis was performed by one-way ANOVA or two-sided unpaired Student's t test. (G) Kaplan-Meier survival curves for cancer-specific survival among patients with HR<sup>+</sup>/HER-2<sup>-</sup> (left, n = 874), patients with HER-2<sup>+</sup> (middle, n = 192), and patients with TNBC (right, n = 241) in the METABRIC dataset. Cases were stratified into two groups according to CD39<sup>+</sup> T<sub>RM</sub> signature enrichment. \*P ≤ 0.05 and \*\*\*\*P ≤ 0.0001. CSS, cancer-specific survival.

expression on dendritic cells and macrophages in the tumor single-cell suspension (fig. S8, A and B). NY-ESO-1-induced proliferation of CD8<sup>+</sup> TILs was observed in CD39<sup>+</sup> T<sub>RM</sub> cells (Fig. 6A), supporting our previous finding that CD39<sup>+</sup> T<sub>RM</sub> cells include tumor-reactive cells. Furthermore, anti-PD-1 with or without anti-CTLA-4 enhanced NY-ESO-1-induced proliferation of CD39<sup>+</sup> T<sub>RM</sub> cells but not CD39<sup>-</sup> T<sub>RM</sub> or non-T<sub>RM</sub> cells. We also performed ex vivo proliferation assays by stimulating CD8<sup>+</sup> TILs from another patient with TNBC with autologous EPCAM<sup>+</sup> tumor cells instead of NY-ESO-1 OLPs and obtained similar results (Fig. 6B).

Next, we stimulated T cells with anti-CD3 in the absence or presence of ICIs using tumor or mLN single-cell suspensions from various molecular subtypes and evaluated the functions of CD8<sup>+</sup> T cells, including the proliferation and production of IFN-γ and TNF-α. Both the cell proliferation and cytokine production of CD8<sup>+</sup> T cells were significantly increased by anti-PD-1 and further enhanced by combination with anti-CTLA-4 (Fig. 6, C and D). In further analysis, we examined the association between enrichment of CD39<sup>+</sup> T<sub>RM</sub> cells and ICI-induced restoration of cytokine production. Two HR<sup>+</sup>/HER-2<sup>-</sup> cases showed low frequencies of CD39<sup>+</sup> T<sub>RM</sub> cells and limited restoration upon anti-PD-1 or

**Fig. 6. CD39<sup>+</sup> T<sub>RM</sub> cells are reinvigorated by blockade of PD-1 and CTLA-4 in vitro. (A and B)** Flow cytometry plots showing reinvigoration of CD39<sup>+</sup> T<sub>RM</sub> cells by ICIs. Sorted CD8<sup>+</sup> TILs from two TNBCs were stimulated in the presence of irradiated autologous feeder cells with NY-ESO-1 OLPs (A) or autologous EPCAM<sup>+</sup> tumor cells (B). After culturing in the absence or presence of anti-PD-1 and/or anti-CTLA-4 for 144 hours, proliferation of each CD8<sup>+</sup> T cell subpopulation was analyzed by CTV dilution and Ki-67 expression. The underlined values in bold represent the frequencies of proliferated CD8<sup>+</sup> T cells among each subpopulation. **(C to E)** Tumor or mLN single-cell suspensions from various molecular subtypes were stimulated with anti-CD3 antibodies in the absence or presence of anti-PD-1 and/or anti-CTLA-4. The proliferation of CD8<sup>+</sup> T cells was analyzed by CTV dilution after 108 hours of culture (HER-2<sup>+</sup> tumors, *n* = 7; TNBC tumors, *n* = 10; TNBC mLN, *n* = 3), and the cytokine production by CD8<sup>+</sup> T cells (HR<sup>+</sup>/HER-2<sup>-</sup> tumors, *n* = 2; HER-2<sup>+</sup> tumors, *n* = 3; TNBC tumors, *n* = 7; TNBC mLN, *n* = 3) was analyzed by intracellular staining of IFN- $\gamma$  and TNF- $\alpha$  after 36 hours. Representative flow cytometry plots are presented in (C). (D) Data are presented as the fold change relative to isotype controls. The mitotic index was calculated as follows: total number of mitotic events divided by absolute number of precursor cells. Wilcoxon matched-pairs signed rank test. (E) Association between the frequencies of CD39<sup>+</sup> T<sub>RM</sub> cells among CD8<sup>+</sup> T cells and ICI-induced restoration of cytokine production. (F) GSEA of up-regulated genes in expanding versus nonexpanding CD8<sup>+</sup> T cells upon neoadjuvant anti-PD-1 treatment in CD39<sup>+</sup> T<sub>RM</sub> and CD39<sup>-</sup> T<sub>RM</sub> cells. The up-regulated gene set was derived from scRNA-seq analyses using pretreatment tumor samples from a clinical trial of neoadjuvant anti-PD-1 treatment in patients with breast cancer (5). **(G)** Ridge plot showing the enrichment score of our CD39<sup>+</sup> T<sub>RM</sub> signature genes in each T cell cluster of breast tumors. scRNA-seq data were obtained from a clinical trial of anti-PD-L1 treatment in patients with TNBC (45). *p* denotes Spearman correlation. *P* values were obtained from two-sided *t* tests. \**P*  $\leq$  0.05, \*\**P*  $\leq$  0.01, and \*\*\**P*  $\leq$  0.001.



anti-PD-1/anti-CTLA-4 treatment. However, HER-2<sup>+</sup> and TNBC cases exhibited broad-range distribution in both the frequency of CD39<sup>+</sup> T<sub>RM</sub> cells and ICI-induced restoration of cytokine production. Overall, the restoration of IFN- $\gamma$  and TNF- $\alpha$  production by anti-PD-1 or anti-PD-1/anti-CTLA-4 treatment significantly correlated with enrichment of CD39<sup>+</sup> T<sub>RM</sub> cells (Fig. 6E). These data implied that CD39<sup>+</sup> T<sub>RM</sub> cells have a capacity for functional restoration upon ICI treatment and may be an ICI-responding subpopulation.

To substantiate our in vitro findings in a clinical setting, we performed GSEA by applying a gene set obtained from a clinical trial of neoadjuvant anti-PD-1 treatment in patients with breast cancer (5) to our bulk RNA-seq data. In this study, the single-cell transcriptomes of expanding versus nonexpanding CD8<sup>+</sup> TILs were analyzed using pretreatment tumors. Up-regulated genes in expanding CD8<sup>+</sup> TILs were significantly enriched in CD39<sup>+</sup> T<sub>RM</sub> cells compared with CD39<sup>-</sup> T<sub>RM</sub> cells (Fig. 6F). We also examined the expression of our CD39<sup>+</sup> T<sub>RM</sub> signature genes in a public scRNA-seq dataset obtained from a clinical trial of anti-PD-L1 treatment in patients with advanced TNBC (45). The single-cell transcriptomes were achieved from breast tumors or metastatic tumors from patients with TNBC treated with chemotherapy alone or in combination with anti-PD-L1 treatment. The CD39<sup>+</sup> T<sub>RM</sub> signature genes were unregulated in CXCL13<sup>+</sup>CD8<sup>+</sup> T cells, which was associated with the response to PD-L1 blockade therapies (fig. S8C and Fig. 6G). Together, these findings provided a rationale for considering ICI blockade of PD-1/PD-L1 and/or CTLA-4 in the treatment of breast cancer, particularly in the presence of CD39<sup>+</sup> T<sub>RM</sub> cell enrichment.

## DISCUSSION

Evaluating the heterogeneity of CD8<sup>+</sup> TILs in the context of tumor specificity and its relationship with systemic immunity is vital to fully understand the antitumor immune responses. Here, we reported that CD39 was expressed in a tumor-specific and exhausted T<sub>RM</sub> subpopulation in both tumors and mLNs. Clonotypes of CD39<sup>+</sup> T<sub>RM</sub> cells systemically overlapped across different compartments. CD39<sup>+</sup> T<sub>RM</sub> cells could be reinvigorated by ICIs, and the restoration of CD8<sup>+</sup> T cell effector functions by ICIs correlated with the relative frequency of CD39<sup>+</sup> T<sub>RM</sub> cells. The CD39<sup>+</sup> T<sub>RM</sub> signature was enriched in TNBC and predicted patient survival. Together, this study provides a better understanding of CD8<sup>+</sup> T cell-mediated antitumor immune responses, especially in terms of systemic immunity, in patients with breast cancer.

Most research in tumor immunology has focused on immune cells in the tumor microenvironment (16, 46–48). However, it is important to know how immune cells in tumor tissues connect to systemic immunity (49–51). Thus, tracking CD8<sup>+</sup> T cell clones across different compartments, including local tissues and peripheral blood, can provide previously unknown insights about systemic antitumor immunity. CD39<sup>+</sup> T<sub>RM</sub> cells in tumors or mLNs were not clonally distinct but overlapped with other CD8<sup>+</sup> T cell subpopulations in the same compartment, revealing a differentiation process of CD8<sup>+</sup> T cells in tissues that was likely induced by encountering tumor antigens. In line with a recent finding that neoantigen-specific CD8<sup>+</sup> T cells are detected in both primary tumors and draining LNs in human NSCLC (52), CD39<sup>+</sup> T<sub>RM</sub> cells were not only clonally

connected but also exhibited shared features between mLNs and primary tumors. In addition, tumor or mLN CD39<sup>+</sup> T<sub>RM</sub> clonotypes, especially with inter-compartmental overlap, were readily detected in T<sub>EM</sub> cells in the peripheral blood, where T<sub>RM</sub> cells hardly exist. This finding suggested that blood T<sub>EM</sub> cells undergo a differentiation process toward CD39<sup>+</sup> T<sub>RM</sub> cells in both tumors and mLNs, requiring further studies. Furthermore, tumor CD39<sup>+</sup> T<sub>RM</sub> clonotypes that have reactivity to autologous tumor cells were detected in blood and mLNs, implying that they not only influence local antitumor immunity but also have importance in systemic antitumor immunity.

Evidence from several types of human solid tumors indicates that bystander CD8<sup>+</sup> T cells that are specific to viral antigens are abundant in tumor tissues (16, 17, 52). However, the presence of bystander CD8<sup>+</sup> TILs in breast cancer has not been investigated. In the current study, we detected CMV- and IAV-specific CD8<sup>+</sup> T cells in breast tumor tissues and peripheral blood and found that those in tumor tissues exhibit T<sub>RM</sub> features. Proof-of-principle studies suggest that tumor-infiltrating CD103<sup>+</sup> T<sub>RM</sub> cells localize in the proximity of breast tumor cells and are associated with a favorable prognosis in patients with TNBC (20, 21, 53). However, IAV-specific CD8<sup>+</sup> T cells in tumor also expressed CD103, and CD103<sup>+</sup> T<sub>RM</sub> cells were detected in tumor-adjacent normal tissue to a similar extent with tumor tissue, implying that a further dissection of CD103<sup>+</sup> T<sub>RM</sub> cells was needed for measurement of antitumor immune responses in breast cancer. We found that most NY-ESO-1-specific CD8<sup>+</sup> TILs coexpressed CD39 and CD103, in contrast to virus-specific CD8<sup>+</sup> TILs, which lacked CD39 expression. The proliferation of CD8<sup>+</sup> T cells responding to OLPs of NY-ESO-1 or autologous tumor cells was observed mostly in CD39<sup>+</sup> T<sub>RM</sub> cells, further supporting their tumor-specific features. In line with tumor-specific features, CD39<sup>+</sup> T<sub>RM</sub> cells in tumors or mLNs were dysfunctional cells with decreased cytokine production and reduced polyfunctionality. Moreover, the CD39<sup>+</sup> T<sub>RM</sub> signature, which was derived from bulk RNA-seq data comparing CD39<sup>+</sup> T<sub>RM</sub> cells with CD39<sup>-</sup> T<sub>RM</sub> cells, was related to better prognosis in TNBCs. Collectively, we confirmed that, in breast cancer, coexpression of CD39 and CD103 provides better understanding of the antitumor immune responses elicited by CD8<sup>+</sup> T cells in tumors or mLNs than CD103 expression.

Patients with breast cancer have distinct risk profiles and pursue different treatment strategies according to the molecular subtype (54). Previous studies have suggested the possibility of a different role of T cell-mediated antitumor immune responses among molecular subtypes (10–15). However, no studies have demonstrated the differences in tumor-infiltrating CD8<sup>+</sup> T cell characteristics among molecular subtypes. In this study, we showed that the enrichment levels of CD39<sup>+</sup> T<sub>RM</sub> cells were significantly different among molecular subtypes. Particularly in HR<sup>+</sup>/HER-2<sup>-</sup> subtypes, tumors included few CD39<sup>+</sup> T<sub>RM</sub> cells, and the enrichment level of the CD39<sup>+</sup> T<sub>RM</sub> gene signature did not have prognostic value in predicting cancer-specific survival, suggesting a limited antitumor immune response elicited by CD8<sup>+</sup> TILs. However, TNBC tumors contained considerable numbers of CD39<sup>+</sup> T<sub>RM</sub> cells, which may be caused by higher immunogenicity compared with other subtypes and can be associated with previous observations of a better response to immunotherapy than other subtypes in clinical trials (55).



Neoadjuvant ICIs enhance antitumor immune responses by eliciting a stronger and broader T cell response compared with adjuvant ICIs in a mouse model or several types of human cancers (56–60). In addition, a single-cell analysis focusing on TCR shows that preexisting T cell clones in tumors can expand after neoadjuvant anti-PD-1 treatment in early breast cancer (5). Considering the known mechanism of ICIs, which reinvigorate tumor antigen-specific exhausted CD8<sup>+</sup> T cells, patient selection based on the enrichment level of CD39<sup>+</sup> T<sub>RM</sub> cells in tumors could be optimal practice for implementing immunotherapy. In the present study, CD39<sup>+</sup> T<sub>RM</sub> cells in tumors from patients with early breast cancer responded to ICIs *in vitro*. Accordingly, active application of neoadjuvant ICIs could be considered in CD39<sup>+</sup> T<sub>RM</sub> cell-enriched tumors. Because CD39<sup>+</sup> T<sub>RM</sub> clonotypes were not only compartmentalized in tumors or mLNs but also clonally connected to peripheral blood, neoadjuvant ICIs may enhance systemic antitumor immunity across multiple compartments. In our *in vitro* functional assays, combined blockade of CTLA-4 and PD-1 showed enhanced efficacy over the blockade of PD-1 alone, justifying the clinical application of combined CTLA-4 and PD-1/PD-L1 blockade for patients with CD39<sup>+</sup> T<sub>RM</sub> cell-enriched breast cancer. In contrast, therapeutic strategies that stimulate antigen priming and tumor infiltration of tumor-specific T cells may precede ICI treatment in the case of CD39<sup>+</sup> T<sub>RM</sub> cells-depleted tumors.

This study has some limitations. First, in the analysis of TCR clonal overlap, a sorted cell population could have been contaminated by unwanted cells, and, thus, minor clonotypes could potentially originate from contaminating cells. We confirmed that the effect of contaminating clonotypes was minimal, but this issue should be considered with caution when interpreting our clonotype analysis. Second, our *in vitro* T cell reinvigoration assays assessed the capacity of T cells for functional restoration in the presence of anti-PD-1 but did not reflect the real *in vivo* responses to anti-PD-1 treatment. Further clinical studies are warranted among ICI-treated patients with breast cancer.

In summary, we dissected the heterogeneity of T<sub>RM</sub> cells in terms of antigen specificity and found the CD39<sup>+</sup> T<sub>RM</sub> subpopulation, which underlies a disparate role of the antitumor immune responses among molecular subtypes of breast cancer. We tracked clonotypes of various CD8<sup>+</sup> T cell subpopulations across multiple compartments, including tumors, mLNs, and blood, revealing the clonal overlap of CD39<sup>+</sup> T<sub>RM</sub> cells with systemic antitumor immunity. Thus, the functional reinvigoration of CD39<sup>+</sup> T<sub>RM</sub> cells upon ICIs offers insights into the feasibility of neoadjuvant ICI treatment, particularly the combination of anti-PD-1/PD-L1 and anti-CTLA-4, in early breast cancer. Last, our findings have potential implications for different immunotherapeutic strategies according to the enrichment level of CD39<sup>+</sup> T<sub>RM</sub> cells.

## MATERIALS AND METHODS

### Study design

The aim of the study was to better understand CD8<sup>+</sup> T cell-mediated antitumor immune responses, especially in terms of systemic immunity, in patients with breast cancer. Using peripheral blood and tissue samples obtained from primary tumors and mLNs, we dissected the heterogeneity of CD8<sup>+</sup> T cells focusing on antigen

specificity and compared phenotypic and transcriptomic features of CD8<sup>+</sup> T cells among different compartments. To understand a systemic aspect of antitumor immunity, we tracked clonotypes of CD39<sup>+</sup> T<sub>RM</sub> cells with tumor-specific features both in and across different compartments. To verify the role of CD39<sup>+</sup> T<sub>RM</sub>-mediated antitumor immune responses in breast cancer, we examined a prognostic value of the CD39<sup>+</sup> T<sub>RM</sub> cell enrichment. *In vitro* functional assays and bioinformatic analysis using public scRNA-seq datasets from clinical trials were performed to assess a capacity for functional restoration of CD39<sup>+</sup> T<sub>RM</sub> cells upon ICI treatment.

### Characteristics of study patients

Clinical samples were prospectively obtained from 131 patients with early breast cancer who underwent surgical resection for curative aim between March 2015 and December 2020 at Severance Hospital, Gangnam Severance Hospital, Seoul St. Mary Hospital, and Daejeon St. Mary Hospital. Clinical and pathological characteristics are presented in table S2. All patients were given sufficient information on the study protocol and provided written informed consent. This study was approved by the Institutional Review Board (IRB) of Severance Hospital (IRB number, 4-2014-0054), Gangnam Severance Hospital (IRB number, 3-2015-0342), Seoul St. Mary Hospital (IRB number, KC18TED10854), and Daejeon St. Mary Hospital (IRB number, DC18TES10068).

### Ethics statement

All patients provided written informed consent after being given sufficient information on the study protocol. This study was carried out in accordance with the Declaration of Helsinki and all procedures approved by the IRB.

### Sample preparation

Adjacent normal and tumor breast tissues and LNs for which metastasis was confirmed by intraoperative frozen section examination were collected from patients. We also collected peripheral venous blood from each patient in sodium-EDTA tubes. Peripheral blood mononuclear cells (PBMCs) were isolated from peripheral venous blood by density gradient centrifugation using lymphocyte separation medium (Corning). Normal breast tissue, tumor breast tissue, and mLNs were mechanically divided into segments using the gentleMACS Dissociator and MACS C-tubes (Miltenyi Biotec) and enzymatically dissociated into single-cell suspensions using the Tumor Dissociation Kit (Miltenyi Biotec) according to the manufacturer's instructions. Dissociated single-cell suspensions were dispersed through a 70- $\mu$ m filter. Isolated PBMCs and single-cell suspensions were cryopreserved in fetal bovine serum (FBS; Corning) with 10% dimethyl sulfoxide (Sigma-Aldrich) and stored in liquid nitrogen at  $-80^{\circ}\text{C}$ . Cryopreserved samples were thawed in a  $37^{\circ}\text{C}$  water bath, and deoxyribonuclease (Thermo Fisher Scientific) was added for 5 min at room temperature. Cells were washed with RPMI 1640 (Corning) + 10% FBS + 1% penicillin-streptomycin. After washing, cells were resuspended in appropriate medium for further experiments.

## Flow cytometry and data analyses

After thawing, dead cells were gated out using the LIVE/DEAD fixable dead cell stain kit (Invitrogen). Cells were washed once by stain buffer (BD Biosciences), stained with fluorochrome-conjugated antibodies against surface protein for 30 min at 4°C, and then washed again. For intracellular staining, the cells were fixed and permeabilized with the Foxp3 staining buffer kit (Thermo Fisher Scientific) and stained with fluorochrome-conjugated antibodies against intracellular protein. The following monoclonal antibodies were used for multicolor flow cytometry: anti-hCD3 BV510 (clone UCHT1, catalog no. 563109, 1:100), anti-hCD3 allophycocyanin (APC; clone HIT3a, catalog no. 300312, 1:100), anti-hCD4 BV605 (clone RPA-T4, catalog no. 562358, 1:100), anti-hCD4 fluorescein isothiocyanate (FITC; clone RPA-T4, catalog no. 555346, 1:100), anti-hCD4 PerCPCy5.5 (clone RPA-T4, catalog no. 560650, 1:100), anti-hCD8 APC-Cy7 (clone SK1, catalog no. 560179, 1:100), anti-hCD8 BV605 (clone SK1, catalog no. 564116, 1:100), anti-hCD8 BV711 (clone RPA-T8, catalog no. 563677, 1:100), anti-hCD8 FITC (clone RPA-T8, catalog no. 301050, 1:100), anti-hCD14 phycoerythrin (PE)-CF594 (clone MφP9, catalog no. 562335, 1:100), anti-hCD14 PE-Cy7 (clone MφP9, catalog no. 562698, 1:100), anti-hCD19 PE-CF594 (clone HIB19, catalog no. 562294, 1:100), anti-hCD69 PE-Cy7 (clone FN50, catalog no. 557745, 1:100), anti-hCD69 PerCPCy5.5 (clone FN50, catalog no. 560738, 1:100), anti-hCD137 APC (clone 4B4-1, catalog no. 550890, 1:100), anti-hCD137 PE (clone 4B4-1, catalog no. 309804, 1:100), anti-hIFN- $\gamma$  PE-Cy7 (clone 4S.B3, catalog no. 557844, 1:100), anti-hIL-2 APC (clone MQ1-17H12, catalog no. 554567, 1:100), anti-hKi-67 BV786 (clone B56, catalog no. 563756, 1:100), anti-hKi-67 BV711 (clone Ki-67, catalog no. 350516, 1:100), anti-hTNF AF700 (clone Mab11, catalog no. 557996, 1:100), anti-hCCR7 PerCPCy5.5 (clone G043H7, catalog no. 353220, 1:100), anti-hCD45RA APC-Cy7 (clone HI100, catalog no. 304128, 1:100), anti-hPD-1 BV421 (clone EH12.2H7, catalog no. 329920, 1:100), anti-hCD103 BB515 (clone Ber-ACT8, catalog no. 564578, 1:100), anti-hCD56 BV786 (clone NCAM16.2, catalog no. 564058, 1:100), anti-hCD11b BV510 (clone ICRF44, catalog no. 563088, 1:100), anti-hCD11c FITC (clone B-ly6, catalog no. 561355, 1:100), anti-hCD15 BV650 (clone HI98, catalog no. 564232, 1:100), anti-hCD39 BB515 (clone Tü66, catalog no. 565469, 1:100), anti-hCD39 BV711 (clone Tü66, catalog no. 563680, 1:100), anti-hCD45 AF700 (clone HI30, catalog no. 560566, 1:100), anti-hTIM-3 BV785 (clone F38-2E2, catalog no. 345031, 1:100), anti-hHLA-DR BV785 (clone L243, catalog no. 307642, 1:100), anti-hCTLA-4 PerCP-eFluor 710 (clone 14D3, catalog no. 46-1529-42, 1:100), anti-hTOX PE (clone TXRX10, catalog no. 12-6502-82, 1:100), anti-hEomes PE-Cy7 (clone WD1928, catalog no. 25-4877-42, 1:100), and anti-hT-bet APC (clone eBio4B10, catalog no. 17-5825-82, 1:100) from BD Biosciences, BioLegend, or Invitrogen. Flow cytometry analyses were performed on an LSR II instrument using FACSDiva software (BD Biosciences). The data were analyzed by FlowJo software (Treestar).

## Multimer staining

After thawing, cells were incubated with dasatinib (50 nM, Sigma-Aldrich) for 15 min at 37°C and then stained with fluorochrome-conjugated HLA-A\*0201 dextramers for NY-ESO-1<sub>157–165</sub> (SLLMWITQV; Immudex) or HLA-A\*0201 pentamers for CMV

pp65<sub>495–503</sub> (NLVPMVATV; Proimmune) or Flu M1<sub>58–66</sub> (GILGFVFTL; Proimmune) for 15 min at room temperature. After washing once by stain buffer, the cells were incubated with purified anti-PE (BioLegend), purified anti-FITC (BioLegend), or anti-APC (BioLegend) antibodies for 15 min at room temperature and then washed again. Surface proteins or intracellular proteins were stained by fluorochrome-conjugated antibodies as above, and flow cytometry analyses were performed.

## RNA-seq and data analyses

After thawing, single-cell suspensions of tumors were enriched using CD8 Microbeads and manual MACS magnetic separators (Miltenyi Biotec) following the manufacturer's instructions. Enriched tumor-infiltrating CD8<sup>+</sup> T cells were sorted into CD103<sup>−</sup>CD39<sup>−</sup>, CD103<sup>+</sup>CD39<sup>−</sup>, and CD103<sup>+</sup>CD39<sup>+</sup> subpopulations using a FACSaria II cell sorter (BD Biosciences). The SMART-Seq v4 Ultra-Low Input RNA kit for sequencing (Takara Bio, USA) was used to extract total RNA, to synthesize cDNA from mRNA, to amplify cDNA, and to construct a library following the manufacturer's instructions. The amplified cDNA quality was validated using an Agilent high sensitivity DNA kit and the Agilent 2100 bioanalyzer. Libraries were pooled, and high-throughput sequencing was performed by paired-end 100 base pair (bp)  $\times$  2 running scale using the HiSeq 2500 (Illumina). Raw reads were trimmed using Trimmomatic v.0.38, and the trimmed reads were aligned to the human genome using HISAT2 v.2.1.0 with default parameters. The aligned reads were used to assemble transcripts and counted using StringTie v.1.3.4d. Read counts were normalized by effective library size and differentially expressed genes (DEGs) determined using R package DESeq2 (61). DEG analysis was performed using a generalized linear model with the Wald statistical test. DEGs were defined by a false discovery rate (FDR) < 0.01 and a log<sub>2</sub> fold change > 1. Clustering of DEGs was performed with unsupervised hierarchical clustering primarily to segregate up-regulated and down-regulated genes. GO biological pathway analysis was conducted with the R package clusterProfiler using up-regulated DEGs in CD39<sup>+</sup> T<sub>RM</sub> cells compared with CD39<sup>−</sup> T<sub>RM</sub> cells, with a Bonferroni correction and an adjusted *P* value of 0.05.

## GSEA and survival analysis using an extra dataset

GSEA was used to assess the enrichment of specific gene sets extracted from previous studies. Up-regulated genes in the CD8<sup>+</sup> T<sub>RM</sub>-like cluster or CD8<sup>+</sup> T<sub>EM</sub>-like cluster were obtained from the previous scRNA-seq analysis using breast tumor samples (data available at <https://doi.org/10.5281/zenodo.1169607> and <https://doi.org/10.5281/zenodo.1170580>) (20). Up-regulated genes in exhausted CD8<sup>+</sup> T cells versus memory CD8<sup>+</sup> T cells were obtained from the previous study using the mouse LCMV model (data available at [www.ncbi.nlm.nih.gov/geo/query/acc.cgi?acc=gse9650](http://www.ncbi.nlm.nih.gov/geo/query/acc.cgi?acc=gse9650)) (38). Up-regulated genes in expanding versus nonexpanding CD8<sup>+</sup> T cells upon neoadjuvant anti-PD-1 treatment were obtained from the previous scRNA-seq analysis using pretreatment tumor samples from a clinical trial of human breast cancer (data available at <https://ega-archive.org/studies/EGAS00001004809>) (5). GSEA was performed using the R package clusterProfiler. The scRNA-seq data for T cells in tumors were obtained from a clinical trial (IMPASSION131 trial) of 22 patients with TNBC who

underwent anti-PD-L1 treatment (data available at [www.ncbi.nlm.nih.gov/geo/query/acc.cgi?acc=GSE169246](http://www.ncbi.nlm.nih.gov/geo/query/acc.cgi?acc=GSE169246)) (45). Enrichment scores for our CD39<sup>+</sup> T<sub>RM</sub> gene signature were calculated in each subpopulation of T cells using the AddModuleScore function of the R package Seurat.

To assess the expression and prognostic value of the CD39<sup>+</sup> T<sub>RM</sub> signature (table S3), we referred to the survival analysis pipeline in the previous paper (20). Gene expression and survival data from the METABRIC dataset (43), TCGA dataset, and GSE46141 (44) (data available at [www.ncbi.nlm.nih.gov/geo/query/acc.cgi?acc=GSE46141](http://www.ncbi.nlm.nih.gov/geo/query/acc.cgi?acc=GSE46141)) were accessed through cBioPortal (62) (data available at [www.cbioportal.org/](http://www.cbioportal.org/)) or Gene Expression Omnibus (63) (data available at [www.ncbi.nlm.nih.gov/geo/](http://www.ncbi.nlm.nih.gov/geo/)) and analyzed in R. Breast cancer samples were classified by molecular subtype based on the expression of hormone receptors and HER-2 receptor. Gene expression from the METABRIC dataset was assessed using Kaplan-Meier survival curves generated by stratifying cases in a 50:50 split based on the ranked signature expression, which was determined using the "sig.score" function in R package geneFu.

### TCR-seq and data analyses

After thawing, PBMCs and single-cell suspensions of tumors and LNs were enriched using CD8 Microbeads and manual MACS magnetic separators (Miltenyi Biotec) following the manufacturer's instructions. Enriched CD8<sup>+</sup> T cells were sorted into various CD8<sup>+</sup> T cell subpopulations using a FACSARIA II cell sorter (BD Biosciences). CD8<sup>+</sup> T cells were primarily sorted into CCR7<sup>+</sup>CD45RA<sup>+</sup> T<sub>N</sub>, CCR7<sup>+</sup>CD45RA<sup>-</sup> T<sub>CM</sub>, CCR7<sup>-</sup>CD45RA<sup>-</sup> T<sub>EM</sub>, and CCR7<sup>-</sup>CD45RA<sup>-</sup> T<sub>EMRA</sub> cells. In tumors and mLNs, CCR7<sup>-</sup>CD45RA<sup>-</sup> T<sub>EM</sub> cells were further sorted into CD103<sup>-</sup>CD39<sup>-</sup>, CD103<sup>+</sup>CD39<sup>-</sup>, and CD103<sup>+</sup>CD39<sup>+</sup> subpopulations. After being sorted by a FACSARIA II cell sorter, diverse CD8<sup>+</sup> T cell subpopulations from tumors, mLNs, and blood were constructed into libraries. Sequencing libraries were prepared using the SMARTer Human TCR a/b Profiling Kit (Takara Bio USA). Briefly, after synthesizing cDNA from extracted mRNA and amplifying the synthesized cDNA, we constructed a library following the manufacturer's instructions. The quality of the amplified cDNA was validated using an Agilent high sensitivity DNA kit and the Agilent 2100 bioanalyzer. Illumina HT indexes were used as indexing adapters. The resulting TCR-α/β libraries were pooled and sequenced on an Illumina MiSeq system (paired-end 150 bp). Raw reads of sequence data were aligned and subsequently assembled by MiXCR with default parameters (64). Extracted TCR-α or TCR-β CDR3 repertoires were analyzed in R version 4.1.0. Detailed information on TCR-seq statistics is given in table S1 and fig. S3A. A distinct CDR3 nucleic acid sequence of the TCR-β chain was considered as a clonotype of CD8<sup>+</sup> T cells in this study. The population diversity of the T cell repertoire was quantified using the Shannon entropy index (65). The degree of clonal overlap between two populations was calculated using the Morisita-Horn overlap index in R package Immunarch (66-67).

### Proliferation assays

After thawing, single-cell suspensions of tumors and LNs rested overnight. We then stained the single-cell suspensions using the CellTrace Violet (CTV) cell proliferation kit (Thermo Fisher Scientific) according to the manufacturer's instructions to assess cellular

proliferation. Stained cells were seeded in round-bottom 96-well plates (0.2 M per well) and stimulated ex vivo with anti-CD3 antibody (10 ng/ml; clone OKT3; eBioscience). Cells were cultured in RPMI 1640 (Corning) containing 10% FBS and 1% penicillin-streptomycin. For the T cell restoration assay, anti-PD-1 antibody (10 μg/ml; BioLegend) and/or anti-CTLA-4 antibody (10 μg/ml; BioLegend) was added. For the control well, mouse immunoglobulin G1 (IgG1) isotype control antibody (10 μg/ml; BioLegend) was added. After 108 hours, the cells were harvested, and the dilution of CTV was measured by flow cytometry. The mitotic index was calculated by dividing the total number of mitotic events by the absolute number of precursor cells.

For tumor-specific stimulation, tumor cells were depleted from single-cell suspensions of tumors using CD326 (EPCAM) Microbeads and manual MACS magnetic separators (Miltenyi Biotec). CD8<sup>+</sup> TILs were then isolated from tumor-depleted single-cell suspensions using CD8 Microbeads and manual MACS magnetic separators (Miltenyi Biotec), and remnant single-cell suspensions were irradiated for use as feeder cells. Isolated CD8<sup>+</sup> TILs were stained with CTV, seeded in 96-well plates (0.1 to 0.2 M per well), and stimulated with NY-ESO-1 OLPs (1 μg/ml per peptide, JPT Peptide Technologies) or autologous tumor cells (0.1 to 0.2 M per well) in the presence of irradiated feeder cells (0.1 to 0.2 M per well). Cells were cultured in RPMI 1640 (Corning) containing 10% FBS and 1% penicillin-streptomycin. For T cell restoration assays, anti-PD-1 antibody and/or anti-CTLA-4 antibody was added. For the control well, mouse IgG1 isotype control antibody (10 μg/ml; BioLegend) was added. After incubation for 144 hours, CD8<sup>+</sup> TILs were harvested and proliferation measured as indicated above.

### Intracellular cytokine staining

For cytokine production assays, single-cell suspensions of tumors and LNs that had rested overnight or sorted subpopulations of CD8<sup>+</sup> TILs (CD39<sup>+</sup>CD103<sup>+</sup>, CD39<sup>-</sup>CD103<sup>+</sup>, and CD39<sup>-</sup>CD103<sup>-</sup>) were seeded in 96-well plates (0.2 M per well) and stimulated ex vivo with anti-CD3 antibody (10 μg/ml; clone OKT3, eBioscience). Cells were cultured with brefeldin A (1:1000; BD Biosciences) and monensin (1:1000; BD Biosciences) in RPMI 1640 (Corning) containing 10% FBS and 1% penicillin-streptomycin. After 6 hours, cells were harvested and stained with fluorochrome-conjugated antibodies against surface markers. After being fixed and permeabilized, cells were stained with fluorochrome-conjugated anti-IFN-γ, anti-TNF-α, or IL-2 antibodies, and cytokine production was measured by flow cytometry.

For T cell restoration assays, single-cell suspensions of tumors and LNs were thawed and rested overnight. The single-cell suspensions were then seeded in 96-well plates (0.2 M per well) and stimulated ex vivo with anti-CD3 antibody (10 μg/ml; clone OKT3, eBioscience). Anti-PD-1 antibody (10 μg/ml; BioLegend) and/or anti-CTLA-4 antibody (10 μg/ml; BioLegend) was added, and mouse IgG1 isotype control antibody (10 μg/ml; BioLegend) was added to a control well. After 24 hours, cells were incubated with brefeldin A (1:1000; BD Biosciences) and monensin (1:1000; BD Biosciences). After another 12 hours, cells were harvested and stained with fluorochrome-conjugated antibodies against surface markers. After being fixed and permeabilized, cells were stained with fluorochrome-conjugated anti-IFN-γ, anti-TNF-α, or IL-2



antibodies, and cytokine production was measured by flow cytometry.

### Statistics and reproducibility

Categorical data are presented as frequencies with percentages. Continuous data are presented as means with SDs. The intergroup differences were analyzed using the unpaired Student's *t* test or Mann-Whitney *U* test depending on whether the data satisfied the assumption of a normal distribution. The paired Student's *t* test or Wilcoxon signed-rank test was used to compare matched samples depending on whether the data satisfied the assumption of a normal distribution. One-way analysis of variance (ANOVA) was used to compare parametric data between multiple unpaired groups. Kaplan-Meier survival curves were analyzed by two-sided log-rank tests. All tests were two-sided.  $P < 0.05$  was considered significant, and confidence intervals were calculated at the 95th percentile. For all statistical tests involving multiple comparisons, an FDR-adjusted  $P < 0.05$  was considered significant. GraphPad Prism version 7 (GraphPad Software, La Jolla, CA) or R (version 4.1.0) was used for statistical analyses and to present the analyzed data as graphs. In flow cytometry, if there were fewer than 100 events of gated subpopulations, data were excluded from the analyses. Otherwise, no data were excluded from the analyses. No statistical method was used to predetermine sample sizes. Experiments were not randomized, and investigators were not blinded. Experiments did not include replicates because all participants and their data are unique.

### Supplementary Materials

#### This PDF file includes:

Figs. S1 to S8  
Tables S1 to S3

#### Other Supplementary Material for this manuscript includes the following:

Table S4

[View/request a protocol for this paper from Bio-protocol.](#)

### REFERENCES AND NOTES

- P. Schmid, S. Adams, H. S. Rugo, A. Schneeweiss, C. H. Barrios, H. Iwata, V. Dieras, R. Hegg, S. A. Im, G. Shaw Wright, V. Henschel, L. Molinero, S. Y. Chui, R. Funke, A. Husain, E. P. Winer, S. Loi, L. A. Emens; IMpassion130 Trial Investigators, Atezolizumab and Nab-paclitaxel in advanced triple-negative breast cancer. *N. Engl. J. Med.* **379**, 2108–2121 (2018).
- T. Bachelot, T. Filleron, I. Bieche, M. Arnedos, M. Campone, F. Dalenc, F. Coussy, M. P. Sablin, M. Debled, C. Lefeuvre-Plesse, A. Goncalves, M. M. Reynier, W. Jacot, B. You, P. Barthelemy, B. Verret, N. Isambert, X. Tchiknavorian, C. Levy, J. C. Thery, T. L'Haridon, J. M. Ferrero, A. Mege, F. Del Piano, E. Rouleau, A. Tran-Dien, J. Adam, A. Lusque, M. Jimenez, A. Jacquet, I. Garberis, F. Andre, Durvalumab compared to maintenance chemotherapy in metastatic breast cancer: The randomized phase II SAFIRO2-BREAST IMMUNO trial. *Nat. Med.* **27**, 250–255 (2021).
- P. Schmid, J. Cortes, L. Pusztai, H. McArthur, S. Kummel, J. Bergh, C. Denkert, Y. H. Park, R. Hui, N. Harbeck, M. Takahashi, T. Foukakis, P. A. Fasching, F. Cardoso, M. Untch, L. Jia, V. Karantz, J. Zhao, G. Aktan, R. Dent, J. O'Shaughnessy; KEYNOTE-522 Investigators, Pembrolizumab for early triple-negative breast cancer. *N. Engl. J. Med.* **382**, 810–821 (2020).
- S. Loibl, M. Untch, N. Burchardi, J. Huober, B. V. Sinn, J. U. Blohmer, E. M. Grischke, J. Furlanetto, H. Tesch, C. Hanusch, K. Engels, M. Rezaei, C. Jackisch, W. D. Schmitt, G. von Minckwitz, J. Thomalla, S. Kummel, B. Rautenberg, P. A. Fasching, K. Weber, K. Rhiem, C. Denkert, A. Schneeweiss, A randomised phase II study investigating durvalumab in addition to an anthracycline taxane-based neoadjuvant therapy in early triple-negative breast cancer: Clinical results and biomarker analysis of GeparNuevo study. *Ann. Oncol.* **30**, 1279–1288 (2019).
- A. Bassez, H. Vos, L. Van Dyck, G. Floris, I. Arijis, C. Desmedt, B. Boeckx, M. Vanden Bempt, I. Nevelsteen, K. Lambein, K. Punie, P. Neven, A. D. Garg, H. Wildiers, J. Qian, A. Smeets, D. Lambrechts, A single-cell map of intratumoral changes during anti-PD1 treatment of patients with breast cancer. *Nat. Med.* **27**, 820–832 (2021).
- H. S. Rugo, J. P. Delord, S. A. Im, P. A. Ott, S. A. Piha-Paul, P. L. Bedard, J. Sachdev, C. Le Tourneau, E. M. J. van Brummelen, A. Varga, R. Salgado, S. Loi, S. Saraf, D. Pietrangelo, V. Karantz, A. R. Tan, Safety and antitumor activity of pembrolizumab in patients with estrogen receptor-positive/human epidermal growth factor receptor 2-negative advanced breast cancer. *Clin. Cancer Res.* **24**, 2804–2811 (2018).
- L. Wein, S. J. Luen, P. Savas, R. Salgado, S. Loi, Checkpoint blockade in the treatment of breast cancer: Current status and future directions. *Br. J. Cancer* **119**, 4–11 (2018).
- E. Krasniqi, G. Barchiesi, L. Pizzuti, M. Mazzotta, A. Venuti, M. Maugeri-Sacca, G. Sanguineti, G. Massimiani, D. Sergi, S. Carpano, P. Marchetti, S. Tomao, T. Gamucci, R. De Maria, F. Tomao, C. Natoli, N. Tinari, G. Ciliberto, M. Barba, P. Vici, Immunotherapy in HER2-positive breast cancer: State of the art and future perspectives. *J. Hematol. Oncol.* **12**, 111 (2019).
- B. Vogelstein, N. Papadopoulos, V. E. Velculescu, S. Zhou, L. A. Diaz Jr., K. W. Kinzler, Cancer genome landscapes. *Science* **339**, 1546–1558 (2013).
- S. Luen, B. Virasamy, P. Savas, R. Salgado, S. Loi, The genomic landscape of breast cancer and its interaction with host immunity. *Breast* **29**, 241–250 (2016).
- S. E. Stanton, S. Adams, M. L. Disis, Variation in the incidence and magnitude of tumor-infiltrating lymphocytes in breast cancer subtypes: A systematic review. *JAMA Oncol.* **2**, 1354–1360 (2016).
- S. Loi, N. Sirtaine, F. Piette, R. Salgado, G. Viale, F. Van Eenoo, G. Rouas, P. Francis, J. P. Crown, E. Hitre, E. de Azambuja, E. Quinaux, A. Di Leo, S. Michiels, M. J. Piccart, C. Sotiriou, Prognostic and predictive value of tumor-infiltrating lymphocytes in a phase III randomized adjuvant breast cancer trial in node-positive breast cancer comparing the addition of docetaxel to doxorubicin with doxorubicin-based chemotherapy: BIG 02-98. *J. Clin. Oncol.* **31**, 860–867 (2013).
- S. Loi, S. Michiels, R. Salgado, N. Sirtaine, V. Jose, D. Fumagalli, P. L. Kellokumpu-Lehtinen, P. Bono, V. Kataja, C. Desmedt, M. J. Piccart, S. Loibl, C. Denkert, M. J. Smyth, H. Joensuu, C. Sotiriou, Tumor infiltrating lymphocytes are prognostic in triple negative breast cancer and predictive for trastuzumab benefit in early breast cancer: Results from the FinHER trial. *Ann. Oncol.* **25**, 1544–1550 (2014).
- H. R. Ali, E. Provenzano, S. J. Dawson, F. M. Blows, B. Liu, M. Shah, H. M. Earl, C. J. Poole, L. Hiller, J. A. Dunn, S. J. Bowden, C. Twelves, J. M. Bartlett, S. M. Mahmoud, E. Rakha, I. O. Ellis, S. Liu, D. Gao, T. O. Nielsen, P. D. Pharoah, C. Caldas, Association between CD8<sup>+</sup> T-cell infiltration and breast cancer survival in 12,439 patients. *Ann. Oncol.* **25**, 1536–1543 (2014).
- C. Denkert, G. von Minckwitz, S. Darb-Esfahani, B. Lederer, B. I. Heppner, K. E. Weber, J. Budczies, J. Huober, F. Klauschen, J. Furlanetto, W. D. Schmitt, J.-U. Blohmer, T. Karn, B. M. Pfitzner, S. Kümmel, K. Engels, A. Schneeweiss, A. Hartmann, A. Noske, P. A. Fasching, C. Jackisch, M. van Mackelenbergh, P. Sinn, C. Schem, C. Hanusch, M. Untch, S. Loibl, Tumour-infiltrating lymphocytes and prognosis in different subtypes of breast cancer: A pooled analysis of 3771 patients treated with neoadjuvant therapy. *Lancet Oncol.* **19**, 40–50 (2018).
- W. Scheper, S. Kelderman, L. F. Fanchi, C. Linnemann, G. Bendle, M. A. J. de Rooij, C. Hirt, R. Mezzadra, M. Slagter, R. Dijkstra, R. J. C. Kluin, P. Snaebjornsson, K. Milne, B. H. Nelson, H. Zijlmans, G. Kenter, E. E. Voest, J. Haanen, T. N. Schumacher, Low and variable tumor reactivity of the intratumoral TCR repertoire in human cancers. *Nat. Med.* **25**, 89–94 (2019).
- Y. Simoni, E. Becht, M. Fehlings, C. Y. Loh, S. L. Koo, K. W. Teng, J. P. S. Yeong, R. Nahar, T. Zhang, H. Kared, K. Duan, N. Ang, M. Poidinger, Y. Y. Lee, A. Larbi, A. J. Khng, E. Tan, C. Fu, R. Mathew, M. Teo, W. T. Lim, C. K. Toh, B. H. Ong, T. Koh, A. M. Hillmer, A. Takano, T. K. H. Lim, E. H. Tan, W. Zhai, D. S. W. Tan, I. B. Tan, E. W. Newell, Bystander CD8<sup>+</sup> T cells are abundant and phenotypically distinct in human tumour infiltrates. *Nature* **557**, 575–579 (2018).
- A. P. Ganesan, J. Clarke, O. Wood, E. M. Garrido-Martin, S. J. Chee, T. Mellows, D. Samaniego-Castruita, D. Singh, G. Seumo, A. Alzetani, E. Woo, P. S. Friedmann, E. V. King, G. J. Thomas, T. Sanchez-Elsner, P. Vijayanand, C. H. Ottensmeier, Tissue-resident memory features are linked to the magnitude of cytotoxic T cell responses in human lung cancer. *Nat. Immunol.* **18**, 940–950 (2017).

19. J. R. Webb, K. Milne, P. Watson, R. J. Deleeuw, B. H. Nelson, Tumor-infiltrating lymphocytes expressing the tissue resident memory marker CD103 are associated with increased survival in high-grade serous ovarian cancer. *Clin. Cancer Res.* **20**, 434–444 (2014).
20. P. Savas, B. Virassamy, C. Ye, A. Salim, C. P. Mintoff, F. Caramia, R. Salgado, D. J. Byrne, Z. L. Teo, S. Dushyanthen, A. Byrne, L. Wein, S. J. Luen, C. Poliness, S. S. Nightingale, A. S. Skandarajah, D. E. Gyorki, C. M. Thornton, P. A. Beavis, S. B. Fox; Kathleen Cuninghame Foundation Consortium for Research into Familial Breast Cancer (kConFab), P. K. Darcy, T. P. Speed, L. K. Mackay, P. J. Neeson, S. Loi, Single-cell profiling of breast cancer T cells reveals a tissue-resident memory subset associated with improved prognosis. *Nat. Med.* **24**, 986–993 (2018).
21. C. A. Egelston, C. Avalor, T. Y. Tu, A. Rosario, R. Wang, S. Solomon, G. Srinivasan, M. S. Nelson, Y. Huang, M. H. Lim, D. L. Simons, T. F. He, J. H. Yim, L. Kruper, J. Mortimer, S. Yost, W. Guo, C. Ruel, P. H. Frankel, Y. Yuan, P. P. Lee, Resident memory CD8<sup>+</sup> T cells within cancer islands mediate survival in breast cancer patients. *JCI Insight* **4**, e130000 (2019).
22. T. Duhen, R. Duhen, R. Montler, J. Moses, T. Moudgil, N. F. de Miranda, C. P. Goodall, T. C. Blair, B. A. Fox, J. E. McDermott, S. C. Chang, G. Grunkemeier, R. Leidner, R. B. Bell, A. D. Weinberg, Co-expression of CD39 and CD103 identifies tumor-reactive CD8 T cells in human solid tumors. *Nat. Commun.* **9**, 2724 (2018).
23. C. M. Laumont, M. C. A. Wouters, J. Smazynski, N. S. Gierc, E. A. Chavez, L. C. Chong, S. Thornton, K. Milne, J. R. Webb, C. Steidl, B. H. Nelson, Single-cell profiles and prognostic impact of tumor-infiltrating lymphocytes coexpressing CD39, CD103, and PD-1 in ovarian cancer. *Clin. Cancer Res.* **27**, 4089–4100 (2021).
24. M. A. Eiva, D. K. Omran, J. A. Chacon, D. J. Powell Jr., Systematic analysis of CD39, CD103, CD137, and PD-1 as biomarkers for naturally occurring tumor antigen-specific TILs. *Eur. J. Immunol.* **52**, 96–108 (2022).
25. G. Leem, J. Park, M. Jeon, E. S. Kim, S. W. Kim, Y. J. Lee, S. J. Choi, B. Choi, S. Park, Y. S. Ju, I. Jung, S. Kim, E. C. Shin, J. Y. Lee, S. H. Park, 4-1BB co-stimulation further enhances anti-PD-1-mediated reinvigoration of exhausted CD39<sup>+</sup> CD8 T cells from primary and metastatic sites of epithelial ovarian cancers. *J. Immunother. Cancer* **8**, e001650 (2020).
26. F. P. Canale, M. C. Ramello, N. Núñez, C. L. Araujo Furlan, S. N. Bossio, M. Gorosito Serrán, J. Tosello Boari, A. Del Castillo, M. Ledesma, C. Sedlik, E. Piaggio, A. Gruppi, E. A. Acosta Rodríguez, C. L. Montes, CD39 expression defines cell exhaustion in tumor-infiltrating CD8<sup>+</sup> T cells. *Cancer Res.* **78**, 115–128 (2018).
27. P. K. Gupta, J. Godec, D. Wolski, E. Adland, K. Yates, K. E. Pauken, C. Cosgrove, C. Ledderose, W. G. Junger, S. C. Robson, E. J. Wherry, G. Alter, P. J. Goulder, P. Klennerman, A. H. Sharpe, G. M. Lauer, W. N. Haining, CD39 expression identifies terminally exhausted CD8<sup>+</sup> T cells. *PLoS Pathog.* **11**, e1005177 (2015).
28. B. C. Miller, D. R. Sen, R. Al Abosy, K. Bi, Y. V. Virkud, M. W. LaFleur, K. B. Yates, A. Lako, K. Felt, G. S. Naik, M. Manos, E. Gjini, J. R. Kuchroo, J. J. Ishizuka, J. L. Collier, G. K. Griffin, S. Maleri, D. E. Comstock, S. A. Weiss, F. D. Brown, A. Panda, M. D. Zimmer, R. T. Manguso, F. S. Hodi, S. J. Rodig, A. H. Sharpe, W. N. Haining, Subsets of exhausted CD8<sup>+</sup> T cells differentially mediate tumor control and respond to checkpoint blockade. *Nat. Immunol.* **20**, 326–336 (2019).
29. Y. Qi, Y. Xia, Z. Lin, Y. Qu, Y. Qi, Y. Chen, Q. Zhou, H. Zeng, J. Wang, Y. Chang, Q. Bai, Y. Wang, Y. Zhu, L. Xu, L. Chen, Y. Kong, W. Zhang, B. Dai, L. Liu, J. Guo, J. Xu, Tumor-infiltrating CD39<sup>+</sup>CD8<sup>+</sup> T cells determine poor prognosis and immune evasion in clear cell renal cell carcinoma patients. *Cancer Immunol. Immunother.* **69**, 1565–1576 (2020).
30. J. Yeong, L. Suteja, Y. Simoni, K. W. Lau, A. C. Tan, H. H. Li, S. Lim, J. H. Loh, F. Y. T. Wee, S. N. Nerurkar, A. Takano, E. H. Tan, T. K. H. Lim, E. W. Newell, D. S. W. Tan, Intratumoral CD39<sup>+</sup>CD8<sup>+</sup> T cells predict response to programmed cell death protein-1 or programmed death ligand-1 blockade in patients With NSCLC. *J. Thorac. Oncol.* **16**, 1349–1358 (2021).
31. M. Sade-Feldman, K. Yizhak, S. L. Bjorgaard, J. P. Ray, C. G. de Boer, R. W. Jenkins, D. J. Lieb, J. H. Chen, D. T. Frederick, M. Barzilay-Rokni, S. S. Freeman, A. Reuben, P. J. Hoover, A. C. Villani, E. Ivanova, A. Portell, P. H. Lizotte, A. R. Aref, J. P. Eliane, M. R. Hammond, H. Vitzthum, S. M. Blackmon, B. Li, V. Gopalakrishnan, S. M. Reddy, Z. A. Cooper, C. P. Paweletz, D. A. Barbie, A. Stemmer-Rachamimov, K. T. Flaherty, J. A. Wargo, G. M. Boland, R. J. Sullivan, G. Getz, N. Hacohen, Defining T cell states associated with response to checkpoint immunotherapy in melanoma. *Cell* **176**, 404 (2019).
32. F. O. Ademuyiwa, W. Bshara, K. Attwood, C. Morrison, S. B. Edge, A. R. Karpf, S. A. James, C. B. Ambrosone, T. L. O'Connor, E. G. Levine, A. Miliotto, E. Ritter, G. Ritter, S. Gnjatich, K. Odunsi, NY-ESO-1 cancer testis antigen demonstrates high immunogenicity in triple negative breast cancer. *PLoS ONE* **7**, e38783 (2012).
33. A. Tessari, L. Pilla, D. Silvia, M. Duca, B. Paolini, M. L. Carcangiu, L. Mariani, F. G. de Braud, S. Cresta, Expression of NY-ESO-1, MAGE-A3, PRAME and WT1 in different subgroups of breast cancer: An indication to immunotherapy? *Breast* **42**, 68–73 (2018).
34. O. Khan, J. R. Giles, S. McDonald, S. Manne, S. F. Ngwi, K. P. Patel, M. T. Werner, A. C. Huang, K. A. Alexander, J. E. Wu, J. Attanasio, P. Yan, S. M. George, B. Bengsch, R. P. Staup, G. Donahue, W. Xu, R. K. Amaravadi, X. Xu, G. C. Karakousis, T. C. Mitchell, L. M. Schuchter, J. Kaye, S. L. Berger, E. J. Wherry, TOX transcriptionally and epigenetically programs CD8<sup>+</sup> T cell exhaustion. *Nature* **571**, 211–218 (2019).
35. A. C. Scott, F. Dunder, P. Zumbo, S. S. Chandran, C. A. Klebanoff, M. Shakiba, P. Trivedi, L. Menocal, H. Appleby, S. Camara, D. Zamarin, T. Walthers, A. Snyder, M. R. Femia, E. A. Comen, H. Y. Wen, M. D. Hellmann, N. Anandasabapathy, Y. Liu, N. K. Altorki, P. Lauer, O. Levy, M. S. Glickman, J. Kaye, D. Betel, M. Philip, A. Schietinger, TOX is a critical regulator of tumour-specific T cell differentiation. *Nature* **571**, 270–274 (2019).
36. C. Yao, H. W. Sun, N. E. Lacey, Y. Ji, E. A. Moseman, H. Y. Shih, E. F. Heuston, M. Kirby, S. Anderson, J. Cheng, O. Khan, R. Handon, J. Reilly, J. Fioravanti, J. Hu, S. Gossa, E. J. Wherry, L. Gattinoni, D. B. McGavern, J. J. O'Shea, P. L. Schwartzberg, T. Wu, Single-cell RNA-seq reveals TOX as a key regulator of CD8<sup>+</sup> T cell persistence in chronic infection. *Nat. Immunol.* **20**, 890–901 (2019).
37. F. Alfei, K. Kanev, M. Hofmann, M. Wu, H. E. Ghoneim, P. Roelli, D. T. Utzschneider, M. von Hoesslin, J. G. Cullen, Y. Fan, V. Eisenberg, D. Wohlleber, K. Steiger, D. Merkler, M. Delorenzi, P. A. Knolle, C. J. Cohen, R. Thimme, B. Youngblood, D. Zehn, TOX reinforces the phenotype and longevity of exhausted T cells in chronic viral infection. *Nature* **571**, 265–269 (2019).
38. E. J. Wherry, S. J. Ha, S. M. Kaech, W. N. Haining, S. Sarkar, V. Kalia, S. Subramaniam, J. N. Blattman, D. L. Barber, R. Ahmed, Molecular signature of CD8<sup>+</sup> T cell exhaustion during chronic viral infection. *Immunity* **27**, 670–684 (2007).
39. M. Larsen, D. Sauce, L. Arnaud, S. Fastenackels, V. Appay, G. Gorochov, Evaluating cellular polyfunctionality with a novel polyfunctionality index. *PLOS ONE* **7**, e24203 (2012).
40. M. D. Martin, V. P. Badovinac, Defining memory CD8 T cell. *Front. Immunol.* **9**, 2692 (2018).
41. F. Sallusto, D. Lenig, R. Förster, M. Lipp, A. Lanzavecchia, Two subsets of memory T lymphocytes with distinct homing potentials and effector functions. *Nature* **401**, 708–712 (1999).
42. P. Romero, A. Zippelius, I. Kurth, M. J. Pittet, C. Touvrey, E. M. Iancu, P. Corthesy, E. Devereux, D. E. Speiser, N. Rufer, Four functionally distinct populations of human effector-memory CD8<sup>+</sup> T lymphocytes. *J. Immunol.* **178**, 4112–4119 (2007).
43. C. Curtis, S. P. Shah, S. F. Chin, G. Turashvili, O. M. Rueda, M. J. Dunning, D. Speed, A. G. Lynch, S. Samarajiva, Y. Yuan, S. Graf, G. Ha, G. Haffari, A. Bashashati, R. Russell, S. McKinney; METABRIC Group, A. Langerod, A. Green, E. Provenzano, G. Wishart, S. Pinder, P. Watson, F. Markowitz, L. Murphy, I. Ellis, A. Purushotham, A. L. Borresen-Dale, J. D. Brenton, S. Tavare, C. Caldas, S. Aparicio, The genomic and transcriptomic architecture of 2,000 breast tumours reveals novel subgroups. *Nature* **486**, 346–352 (2012).
44. S. Kimbung, A. Kovács, P. O. Bendahl, P. Malmström, M. Fernö, T. Hatschek, I. Hedenfalk, Claudin-2 is an independent negative prognostic factor in breast cancer and specifically predicts early liver recurrences. *Mol. Oncol.* **8**, 119–128 (2014).
45. Y. Zhang, H. Chen, H. Mo, X. Hu, R. Gao, Y. Zhao, B. Liu, L. Niu, X. Sun, X. Yu, Y. Wang, Q. Chang, T. Gong, X. Guan, T. Hu, T. Qian, B. Xu, F. Ma, Z. Zhang, Z. Liu, Single-cell analyses reveal key immune cell subsets associated with response to PD-L1 blockade in triple-negative breast cancer. *Cancer Cell* **39**, 1578–1539.e8 (2021).
46. M. Binnewies, E. W. Roberts, K. Kersten, V. Chan, D. F. Fearon, M. Merad, L. M. Coussens, D. I. Gabrilovich, S. Ostrand-Rosenberg, C. C. Hedrick, R. H. Vonderheide, M. J. Pittet, R. K. Jain, W. Zou, T. K. Howcroft, E. C. Woodhouse, R. A. Weinberg, M. F. Krummel, Understanding the tumor immune microenvironment (TIME) for effective therapy. *Nat. Med.* **24**, 541–550 (2018).
47. W. Held, I. Siddiqui, K. Schaeuble, D. E. Speiser, Intratumoral CD8<sup>+</sup> T cells with stem cell-like properties: Implications for cancer immunotherapy. *Sci. Transl. Med.* **11**, eaay6863 (2019).
48. I. Siddiqui, K. Schaeuble, V. Chennupati, A. A. Fuentes Marraco, S. Calderon-Copete, D. Pais Ferreira, S. J. Carmona, L. Scarpellino, D. Gfeller, S. Pradervand, S. A. Luther, D. E. Speiser, W. Held, Intratumoral Tcf1<sup>+</sup>PD-1<sup>+</sup>CD8<sup>+</sup> T cells with stem-like properties promote tumor control in response to vaccination and checkpoint blockade immunotherapy. *Immunity* **50**, 195–211.e10 (2019).
49. K. J. Hiam-Galvez, B. M. Allen, M. H. Spitzer, Systemic immunity in cancer. *Nat. Rev. Cancer* **21**, 345–359 (2021).
50. M. H. Spitzer, Y. Carmi, N. E. Reticker-Flynn, S. S. Kwek, D. Madhiredy, M. M. Martins, P. F. Gherardini, T. R. Prestwood, J. Chabon, S. C. Bendall, L. Fong, G. P. Nolan, E. G. Engleman, Systemic immunity is required for effective cancer immunotherapy. *Cell* **168**, 487–502.e15 (2017).
51. A. K. Molodtsov, N. Khatwani, J. L. Vella, K. A. Lewis, Y. Zhao, J. Han, D. E. Sullivan, T. G. Searles, N. K. Preiss, T. B. Shabaneh, P. Zhang, A. R. Hawkes, B. T. Malik, F. W. Kolling, E. J. Usherwood, S. L. Wong, J. D. Phillips, K. Shirai, C. V. Angeles, S. Yan, T. J. Curiel, Y. H. Huang, C. Cheng, M. J. Turk, Resident memory CD8<sup>+</sup> T cells in regional lymph nodes mediate immunity to metastatic melanoma. *Immunity* **54**, 2117–2132.e7 (2021).
52. J. X. Caushi, J. Zhang, Z. Ji, A. Vaghiasa, B. Zhang, E. H. Hsiue, B. J. Mog, W. Hou, S. Justesen, R. Blosser, A. Tam, Y. Anagnostou, T. R. Cottrell, H. Guo, H. Y. Chan, D. Singh, S. Thapa, A. G. Dykema, P. Burman, B. Choudhury, L. Aparicio, L. S. Cheung, M. Lanis, Z. Belcaid, M. El Asmar, P. B. Illei, R. Wang, J. Meyers, K. Schuebel, A. Gupta, A. Skaist, S. Wheelan, J. Naidoo, K. A. Marrone, M. Brock, J. Ha, E. L. Bush, B. J. Park, M. Bott, D. R. Jones, J. E. Reuss, V. E. Velculescu, J. E. Haft, K. W. Kinzler, S. Zhou, B. Vogelstein, J. M. Taube, M. D. Hellmann, J. R. Brahmer, T. Merghoub, P. M. Forde, S. Yegnasubramanian, H. Ji, D. M. Pardoll,

- K. N. Smith, Transcriptional programs of neoantigen-specific TIL in anti-PD-1-treated lung cancers. *Nature* **596**, 126–132 (2021).
53. Z. Q. Wang, K. Milne, H. Derocher, J. R. Webb, B. H. Nelson, P. H. Watson, CD103 and intratumoral immune response in breast cancer. *Clin. Cancer Res.* **22**, 6290–6297 (2016).
  54. A. G. Waks, E. P. Winer, Breast cancer treatment. A review. *JAMA* **321**, 288–300 (2019).
  55. S. Adams, M. E. Gatti-Mays, K. Kalinsky, L. A. Korde, E. Sharon, L. Amiri-Kordestani, H. Bear, H. L. McArthur, E. Frank, J. Perlmutter, D. B. Page, B. Vincent, J. F. Hayes, J. L. Gulley, J. K. Litton, G. N. Hortobagyi, S. Chia, I. Krop, J. White, J. Sparano, M. L. Disis, E. A. Mittendorf, Current landscape of immunotherapy in breast cancer: A review. *JAMA Oncol.* **5**, 1205–1214 (2019).
  56. M. Chalabi, L. F. Fanchi, K. K. Dijkstra, J. G. Van den Berg, A. G. Aalbers, K. Sikorska, M. Lopez-Yurda, C. Grootsholten, G. L. Beets, P. Snaebjornsson, M. Maas, M. Mertz, V. Veninga, G. Bounova, A. Broeks, R. G. Beets-Tan, T. R. de Wijkerslooth, A. U. van Lent, H. A. Marsman, E. Nuijten, N. F. Kok, M. Kuiper, W. H. Verbeek, M. Kok, M. E. Van Leerdam, T. N. Schumacher, E. E. Voest, J. B. Haanen, Neoadjuvant immunotherapy leads to pathological responses in MMR-proficient and MMR-deficient early-stage colon cancers. *Nat. Med.* **26**, 566–576 (2020).
  57. C. U. Blank, E. A. Rozeman, L. F. Fanchi, K. Sikorska, B. van de Wiel, P. Kvistborg, O. Krijgsman, M. van den Braber, D. Philips, A. Broeks, J. V. van Thienen, H. A. Mallo, S. Adriaansz, S. Ter Meulen, L. M. Pronk, L. G. Grijpink-Ongering, A. Bruining, R. M. Gittelman, S. Warren, H. van Tinteren, D. S. Peeper, J. Haanen, A. C. J. van Akkooi, T. N. Schumacher, Neoadjuvant versus adjuvant ipilimumab plus nivolumab in macroscopic stage III melanoma. *Nat. Med.* **24**, 1655–1661 (2018).
  58. T. F. Cloughesy, A. Y. Mochizuki, J. R. Orpilla, W. Hugo, A. H. Lee, T. B. Davidson, A. C. Wang, B. M. Ellingson, J. A. Rytlewski, C. M. Sanders, E. S. Kawaguchi, L. Du, G. Li, W. H. Yong, S. C. Gaffey, A. L. Cohen, I. K. Mellinshoff, E. Q. Lee, D. A. Reardon, B. J. O'Brien, N. A. Butowski, P. L. Nghiemphu, J. L. Clarke, I. C. Arrillaga-Romany, H. Colman, T. J. Kaley, J. F. de Groot, L. M. Liau, P. Y. Wen, R. M. Prins, Neoadjuvant anti-PD-1 immunotherapy promotes a survival benefit with intratumoral and systemic immune responses in recurrent glioblastoma. *Nat. Med.* **25**, 477–486 (2019).
  59. T. Cascone, W. N. William Jr., A. Weissferdt, C. H. Leung, H. Y. Lin, A. Pataer, M. C. B. Godoy, B. W. Carter, L. Federico, A. Reuben, M. A. W. Khan, H. Dejima, A. Francisco-Cruz, E. R. Parra, L. M. Solis, J. Fujimoto, H. T. Tran, N. Kalhor, F. V. Fossella, F. E. Mott, A. S. Tsao, G. Blumenschein Jr., X. Le, J. Zhang, F. Skoulidis, J. M. Kurie, M. Altan, C. Lu, B. S. Glisson, L. A. Byers, Y. Y. Elamin, R. J. Mehran, D. C. Rice, G. L. Walsh, W. L. Hofstetter, J. A. Roth, M. B. Antonoff, H. Kadara, C. Haymaker, C. Bernatchez, N. J. Ajami, R. R. Jenq, P. Sharma, J. P. Allison, A. Futreal, J. A. Wargo, I. I. Wistuba, S. G. Swisher, J. J. Lee, D. L. Gibbons, A. A. Vaporciyan, J. V. Heymach, B. Sepesi, Neoadjuvant nivolumab or nivolumab plus ipilimumab in operable non-small cell lung cancer: The phase 2 randomized NEOSTAR trial. *Nat. Med.* **27**, 504–514 (2021).
  60. J. Liu, S. J. Blake, M. C. Yong, H. Harjunpaa, S. F. Ngiew, K. Takeda, A. Young, J. S. O'Donnell, S. Allen, M. J. Smyth, M. W. Teng, Improved efficacy of neoadjuvant compared to adjuvant immunotherapy to eradicate metastatic disease. *Cancer Discov.* **6**, 1382–1399 (2016).
  61. M. I. Love, W. Huber, S. Anders, Moderated estimation of fold change and dispersion for RNA-seq data with DESeq2. *Genome Biol.* **15**, 550 (2014).
  62. J. Gao, B. A. Aksoy, U. Dogrusoz, G. Dresdner, B. Gross, S. O. Sumer, Y. Sun, Integrative analysis of complex cancer genomics and clinical profiles using the cBioPortal. *Sci. Signal.* **6**, pl1 (2013).
  63. T. Barrett, S. E. Wilhite, P. Ledoux, C. Evangelista, I. F. Kim, M. Tomashevsky, K. A. Marshall, NCBI GEO: archive for functional genomics data sets—update. *Nucleic Acids Res.* **41**, D991–D995 (2013).
  64. D. A. Bolotin, S. Poslavsky, I. Mitrophanov, M. Shugay, I. Z. Mamedov, E. V. Putintseva, D. M. Chudakov, *MixCR: software for comprehensive adaptive immunity profiling* Nat Methods **12**, 380–381 (2015).
  65. C. E. Shannon, The mathematical theory of communication. *MD Comput.* **14**, 306–317 (1963).
  66. V. I. Nazarov, M. V. Pogorelyy, E. A. Komech, I. V. Zvyagin, D. A. Bolotin, M. Shugay, D. M. Chudakov, *tcR: an R package for T cell receptor repertoire advanced data analysis.* *BMC Bioinformatics* **16**, 175 (2015).
  67. M. Morisita, Measuring of the dispersion of individuals and analysis of the distributional patterns. *Mem. Fac. Sci. Kyushu Univ., Ser. E (Biol.)* **2**, 215–235 (1959).

## Acknowledgments

We thank San Francisco Edit for editing support.

**Funding:** This study was supported by the National Research Foundation of Korea grants (NRF-2018M3A9D3079498 to E.-C.S. and NRF-2021R111A1A01060331 to J.Y.K.), faculty research grant of Yonsei University College of Medicine (6-2021-0062 to J.Y.K.), and the National Research Foundation of Korea Global Ph.D. Fellowship (NRF-2018H1A2A1063212 to Y.J.L.).

**Author contributions:** Y.J.L., J.Y.K., S.H.J., H.N., S.J.B., J.A., T.-K.Y., W.Y.S., S.G.A., J.J., W.C.P., and S.I.K. were involved in sample acquisition. Y.J.L., J.Y.K., S.H.J., H.N., J.H.J., M.J., and E.-S.K. were involved in data acquisition and analysis. Y.J.L., J.Y.K., S.-H.P., and E.-C.S. were involved in data interpretation and discussion of result. Y.J.L., J.Y.K., and E.-C.S. contributed to the conceptual design of the study. Y.J.L. and E.-C.S. wrote the manuscript.

**Competing interests:** The authors declare that they have no competing interests.

**Data and materials availability:** All analyzed sequencing data are available online. Raw data from the bulk mRNA sequencing were deposited in BioProject under accession number PRJNA779183. Raw data from the bulk TCR-seq data were deposited in BioProject under accession number PRJNA779227. Bioinformatic analyses were performed using open-source software and in-house scripts in R (version 4.1.0), which are available from the corresponding author upon reasonable request. All data needed to evaluate the conclusions in the paper are present in the paper or the Supplementary Materials.

Submitted 23 December 2021

Accepted 21 July 2022

Published 26 August 2022

10.1126/sciimmunol.abn8390